



Published in final edited form as:

Chem Soc Rev. 2016 March 07; 45(5): 1432–1456. doi:10.1039/c5cs00158g.

Simple bioconjugate chemistry serves great clinical advances: albumin as a versatile platform for diagnosis and precision therapy

Zhibo Liu and Xiaoyuan Chen

Laboratory of Molecular Imaging and Nanomedicine, National Institute of Biomedical Imaging and Bioengineering, National Institutes of Health, Bethesda, MD 20892, USA

Abstract

Albumin is the most abundant circulating protein in plasma and has recently emerged as a versatile protein carrier for drug targeting and for improving the pharmacokinetic profile of peptide or protein based drugs. Three drug delivery technologies related to albumin have been developed, which include the coupling of low-molecular weight drugs to exogenous or endogenous albumin, conjugating bioactive proteins by albumin fusion technology (AFT), and encapsulation of drugs into albumin nanoparticles. This review article starts with a brief introduction of human serum albumin (HSA), and then summarizes the mainstream chemical strategies of developing HSA binding molecules for coupling with drug molecules. Moreover, we also concisely condense the recent progress of the most important clinical applications of HSA-binding platforms, and specify the current challenges that need to be met for a bright future of HSA-binding.

1. Introduction

Human serum albumin (HSA) is the most abundant protein in plasma, and it can serve as a versatile carrier for drug delivery as well as for prolonging the active profile of fast-clearance drugs.^{1–3} Besides being a key drug-delivery protein in blood, it also undertakes the transportation of many essential biomolecules, such as fatty acids, hormones and amino acids.^{4,5} HSA has a notably long half-life (19 days) in blood circulation.^{6,7} HSA is produced in the liver cells as preproalbumin, and then modified by Golgi vesicles to give secreted albumin. Approximately 13–14 g of albumin is secreted into the intravascular system each day, and the extravascular HSA will return to intravascular circulation through the lymphatic system.^{8,9} The degradation of HSA is highly dependent on the interaction with albumin receptors, including gp18, gp30, megalin and the neonatal Fc receptor (FcRn).

HSA is widely used as a carrier for small molecule drugs and imaging probes.^{10–19} It is biodegradable and non-toxic and lacks immunogenicity, making it an excellent candidate as an excipient for vaccines and many other pharmaceuticals.^{20,21} In addition, HSA is robust against chemical modifications and can be stable in the pH range of 4–9 at 60 °C for as long as 10 h. Therefore, the amino acid residues on albumin can be readily linked with

therapeutic drugs, imaging reporters and targeting molecules through chemical conjugation. Albumin is also found to specifically target tumor regions because of its enhanced permeability and retention (EPR) effect as well as albumin receptor binding, which is a unique advantage as the carrier for tumor-targeted drug delivery.^{22,23}

There has been long-standing interest in developing a general strategy that can effectively prolong the active profile of pharmaceuticals. Among the currently developed methods, conjugating pharmaceuticals to albumin-binding molecules is one of the most commonly used approaches due to its high efficiency and minimum side effect.²⁴

In the past two decades, a number of advances in HSA-binding therapeutics have been approved by the Food and Drug Administration (FDA), and many more are under active clinical investigation (Table 1). These successful discoveries are of significance to a broad spectrum of healthcare, especially for cancer therapy and diabetes treatment. Overall, the development is often derived from a new understanding of HSA chemistry, followed by a smart application designed to solve an emerging clinical challenge. For instance, the development and market approval of Abraxane, a paclitaxel albumin nanoparticle, became a landmark for both nanomedicine and albumin-based drug delivery technology with annual sales of \$850 million in 2014. Indeed, the thoughts and rationales of these successes are greatly inspiring, not only for the development of future HSA-binding therapeutics, but also to the most general audiences including chemists, biologists and clinical doctors who have interest in new drug development. For a better understanding of these exciting progresses, we would like to share our review to guide the biological design, chemical screening and clinical application of HSA-based drugs, with focus on the strategy of *in vivo* binding that are most practical for clinical use.

2. General strategy to develop HSA-conjugated drugs

2.1. *In vitro* covalent conjugation

To start with, amide coupling based on lysine residue is the most classical method for *in vitro* covalent HSA conjugation (Fig. 1A–D).^{28–34} At present, the functional moieties often contain *p*-isothiocyanate (*p*-SCN) or NHS ester (*N*-hydroxysuccinimide) that can be obtained by *in situ* activation. However, these methods are not site-specific and always lead to a mixture of mono and multiple modified HSA.^{18,19,35–39}

To meet the challenge, an optimized coupling method was developed to perform the conjugation on cysteine-34 instead of lysines on HSA, and has provided better-defined HSA–drug conjugates that have high purity with a constant drug-loading ratio, a minimal alteration of the three-dimensional protein structure and a preset breaking point. However, as the cysteine-34 position on commercially available HSA is largely blocked by cysteine, homocysteine as well as other sulfhydryl containing compounds, the HSA is a mixture of mercaptalbumin and nonmercaptalbumin and only approximately 20–60% of them contain free sulfhydryl groups. To solve this problem, Mansour *et al.* developed a one-step procedure of selectively reducing HSA with dithiothreitol (Cleland's reagent), giving approximately one sulfhydryl group for each HSA molecule (Fig. 1E). In the next step, the reduced HSA is directly coupled with the maleimide modified drugs such as doxorubicin maleimide.

Compared with the free doxorubicin, the HSA-conjugated version was significantly better on curing murine renal carcinoma (RENCA) at equitoxic dose.⁴⁰

In vitro covalent conjugation has been widely used in preparing HSA-based drugs (Fig. 2). For instance, to radiolabel HSA with radiometals for diagnostic imaging, radiometal chelators will be linked on HSA by incubating NHS-activated ester of DOTA (1,4,7,10-tetraazacyclododecane-1,4,7,10-tetraacetic acid) together with HSA under weakly basic conditions (pH = 8–9).^{41,42} ¹⁸F-HSA, ⁶⁸Ga-DOTA-HSA, ¹¹¹In-DTPA-HSA (DTPA is the abbreviation for diethylene triamine pentaacetic acid) and Gd-DTPA-HSA have been considered as blood-pool imaging reagents by using positron emission tomography (PET), single-photon emission computed tomography (SPECT) and magnetic resonance image (MRI), respectively.^{28,43–45} In convention, radioactive HSA is prepared by multiple-step radiosynthesis. Nevertheless, by taking the advantage of the development of milder and more efficient radiolabeling strategies,^{46–50} one-step HSA labeling is likely to be practical in the near future. In addition, peptide and small molecular drugs have also been conjugated on the lysine residues of HSA to develop advanced HSA-binding imaging probe and therapeutics.^{28,43–45}

Fusion protein technology (FPT) is a special way of *in vitro* conjugating HSA with functional moieties yet has been broadly used in preparing recombinant HSA/protein. By doing so, albumin protein conjugates are genetically engineered by putting together the genes of the two molecules and expressing the albumin fusion proteins in yeast strains (Fig. 3).

Clinically, one such albumin fusion protein is Albuferon, a fusion protein of albumin and interferon α -2b for the treatment of hepatitis C.⁵⁹ A number of other albumin fusion proteins have entered early clinical trials. These include fusion proteins with low-molecular weight peptides such as β -natriuretic peptide and glucagon-like peptide 1, as well as fusion proteins with cytokines. Albuleukin, an albumin fusion protein with recombinant interleukin-2 that has shown promising antitumor efficacy against murine renal cell carcinoma and melanoma.^{55,59}

2.2. *In vivo* covalent conjugation

Kratz *et al.* established a strategy that exploits endogenous HSA as a drug carrier.⁶⁰ In this therapeutic strategy, the prodrug binds rapidly and selectively to the cysteine-34 position of circulating serum albumin after intravenous administration thereby generating a macromolecular transport form of the drug *in situ* in the blood. Indeed, the strategy of *in vivo* HSA conjugation would have several advantages over *in vitro* synthesized drug albumin conjugates: (a) the use of commercial and possibly pathogenic albumin is avoided; (b) easy to use and inexpensive to manufacture; and (c) the related quality control is simple, which is comparable to any other low-molecular weight drug candidates.

The macromolecular prodrug approach targets the cysteine-34 position of albumin. A HPLC analysis demonstrates that approximately 70% of circulating albumin in the blood stream is mercaptalbumin (HMA) that contains an accessible cysteine-34.^{4,61,62} Moreover, the free thiol group of cysteine-34 of HSA is an unusual feature of an extracellular protein. As

known, only three other major proteins that contain free cysteine residues in human plasma: (1) apolipoprotein B-100 of low-density lipoprotein (LDL) which has two cysteine residues (Cys-3734 and Cys-4190) located at the C-terminal end of the protein,^{63–65} (2) fibronectin which has two cryptic, free sulfhydryl groups,⁶⁶ and (3) R1-antitrypsin which has a single cysteine residue (Cys-232).^{66–68} However, the sulfhydryl groups in these proteins do not react readily with sulfhydryl reagents under physiological conditions and are normally linked to either cysteine or glutathione in blood circulation. Therefore, the free thiol group on HSA, cysteine-34 of endogenous albumin, is a unique amino acid on the surface of a circulating protein, which is capable of further conjugation.⁶⁹

Proof of concept was obtained with the (6-maleimidocaproyl) hydrazone derivative of doxorubicin (DOXO-EMCH) that rapidly and selectively binds to circulating albumin within a few minutes (Fig. 4). Inspired by translational research with DOXO-EMCH, many albumin-binding prodrugs have been developed (Fig. 5). These prodrugs often consist of an anticancer drug, the maleimide group as the thiol-binding moiety and an enzymatically cleavable peptide linker. Examples include doxorubicin prodrugs that are cleaved by matrix metalloproteases 2 and 9,⁴⁰ cathepsin B,⁷⁰ urokinase plasminogen (uPA) or prostate-specific antigen (PSA),^{71,72} methotrexate prodrugs that are cleaved by cathepsin B or plasmin,⁷³ and camptothecin prodrugs that are cleaved by cathepsin B or unidentified proteases.⁷⁴ In addition, maleimide derivatives with 5-fluorouracil analogues and platinum(II) complexes have been developed.⁷⁵

2.3. *In vitro* non-covalent HSA binding

Besides covalently connecting HSA with small functional molecules, non-covalent van der Waals force or electronic interaction is another approach that can be used for HSA binding.^{79,80} For instance, certain radiometals can form robust conjugates with macro-aggregated albumin (MAA) without using any chelators, the resulting complexes (¹¹¹In-MAA and ^{99m}Tc-MAA, Fig. 6A and B) have been widely used in clinical diagnosis, especially for lung perfusion and for detecting gastrointestinal bleeding by SPECT.^{20,51,81–83} To form this self-assembled capsule, firstly the intramolecular disulfide bonds of HSA are partially reduced by using glutathione (GSH) to give free sulfhydryl groups. Then, the pretreated HSA/ water solution is mixed with small drugs in triaryl butyl alcohol (TBA). Here, TBA is used as the anti-solvent for albumin and water is used as the anti-solvent for the small molecular drugs. In the mixed solution, HSA and small molecular drugs would precipitate out because of the decreased solubility of both HSA and small molecular drugs. At last, this suspension is further incubated at 37 °C to form intermolecular disulfide to give small molecular drug loaded HSA nanoparticles (Fig. 6C).^{20,84}

In addition, *in vitro* non-covalent HSA binding is also commonly used in preparing HSA–nanoparticle complexes, especially for the purpose of imaging and therapy.^{2,26–28,85–90} For instance, IONPs (iron oxide nanoparticles) were incubated with dopamine to become moderately hydrophilic before being doped into HSA matrices *via* non-covalent binding. In this case, a physical capsule is formed between HSA and IONP that can load small molecular drugs with high efficiency. Additionally, as shown in Fig. 6D, the HSA matrix is

capable of carrying fluorophores and radioactive reporters, therefore this type of HSA-binding nanoparticle can serve as a multiple functional platform for the purpose of both *in vivo* imaging and drug delivery.

2.4. *In vivo* non-covalent HSA targeting

The three-dimensional crystal structure of HSA was solved in early 1990s (Fig. 7).⁹² It is a heart-shaped protein with three homogeneous domains, and each domain is composed of two subdomains that own the same structural motifs. Notably, HSA is one of the smallest proteins in human plasma. Both size and abundance explain the fact that the transportation of many metabolic compounds and therapeutic drugs is related to HSA by non-covalent binding. These HSA ligand-binding pockets are a series of hydrophobic cavities in subdomains II and III. Indeed, the design of HSA-binding molecules is mainly based on the structures of binding pockets, which is also the key to determine the physical performance of HSA.

Little was known about the variety of binding sites of HSA until an interesting study was reported in 1975,⁹⁴ which was about the surprisingly different binding affinities of a number of fluorescent molecules for HSA. Changing the side chain on the amino acid moiety of the dansylamino acids was found to substantially affect the binding of these compounds to HSA. In fact, the binding of the dansylamino acids to HSA varied both in the number of binding sites and in the binding tightness to these sites, suggesting that electrostatic and dipolar forces as well as steric factors play a role in both strength and specificity of binding. This study corroborates with the results of Ghuman *et al.*, who figured out based on circular dichroism measurements that the aromatic portion of flufenamic acid was inserted into a hydrophobic crevice on albumin while the carboxylate anion was associated with a cation that is around the gate of a binding pocket.⁹³ Overall, there are two high affinity binding sites for small heterocyclic or aromatic compounds (located on subdomains IIA and IIIA),⁹⁴ two to three dominant long-chain fatty acid binding sites (located on subdomains IB and IIIB), and two distinct metal-binding sites, making a total of six dominant areas of ligand association to albumin.⁹⁵ In this part, we will elaborate on the chemistry of design, synthesis and screening of the small organic albumin-binding entities according to the specific binding sites.

2.4.1. HSA binding site 1—Binding site 1 is an essential pocket of HSA to carry and deliver small molecules in blood circulation. The interior environment of the pocket is predominantly apolar but is composed of two polar residues: an inner one towards the bottom and an outer polar residue near the entrance (Fig. 8). Therefore, the molecules binding to pocket 1 generally contain a lipophilic aromatic structure in the middle and spherically surrounded by negative charges. Many dye molecules bind to domain II with high binding affinities (Table 2).

Among them, Evans blue (EB) dye, as a good example, exhibits high affinity for binding site 1 on serum albumin. EB is an important tool in many physiologic and clinical investigations because of its high affinity for serum albumin, and has been used in clinical practice for almost 90 years as a way of determining patient plasma volume.⁹⁸ By taking advantage of

the high *in vivo* binding affinity of EB to albumin, Niu *et al.* developed a NOTA (1,4,7-triazacyclononane-*N,N*-triacetic acid) conjugate of a truncated form of Evans blue (NEB) for *in vivo* albumin labeling. ^{18}F -labeling was achieved by complexing with ^{18}F -aluminum fluoride (^{18}F -AlF), and ^{68}Ga and ^{64}Cu labeling was accomplished through standard chelation chemistry (Fig. 9).^{99–101}

2.4.2. HSA binding site 2—Different from site 1, binding site 2 has a single main polar patch, located close to one side of the entrance of the binding pocket (Fig. 10). Based on the protein docking study, the hydrophobic binding cleft is about 16 Å deep and about 8 Å wide in the albumin molecule with a cationic group located near the surface. Therefore, as shown in Table 3, most of the binders to site 2 are lipophilic carboxylate derivatives. Nevertheless, a negative charge is not required for the molecule that binds to site 2. For example, diazepam, a basic drug molecule that exists mainly in the un-ionized form at neutral pH, also binds with high affinity for site 2. The presence of a positive charge often precludes binding to site 2. As shown in Table 3, aliphatic amines with chain lengths C-3 to C-12 do not have measurable binding to site 2 although fatty acids with the same side chains are micromolar binders to the same binding pocket.⁹³

Recently, Neri *et al.* reported a class of 4-(*p*-iodophenyl)-butyric acid derivatives that display stable non-covalent interaction with binding site 2. These HSA-binding tags were selected based on the strategy of Systematic Evolution of Ligands by Exponential Enrichment (SELEX). The candidate pool is a DNA-encoded chemical library with more than six hundred oligonucleotide-compound conjugates. After selection, the DNA sequences of stronger albumin binders were amplified by PCR and decoded on oligonucleotide microarrays. The corresponding signal intensities were normalized after selection against the intensities of compounds selected on empty resin (Fig. 11A and B). The selected HSA-binding molecules are listed in Fig. 11C. Interestingly, some of the selected HSA-binding molecules are structurally similar and featured by the basic structure of a 4-phenylbutanoic acid moiety, with different hydrophobic substituents on the phenyl ring (Fig. 11C). Notably, one of these HSA-binding tags has been applied into several pharmaceutical systems to tune their clearance from blood circulation, such as elongation of the pharmaceutical profile of fast clearing drugs (Fig. 11D), improved performance of MRI contrast agents (Fig. 11E), and reduced kidney uptake of radiotherapeutic drugs (Fig. 21).¹⁰³

2.4.3. Fatty acid modification for HSA binding—When Kendall accomplished HSA crystallization in 1941, he found that the product contained a small amount of free fatty acid (FA).¹⁰⁵ In addition, other researchers noted that the lipids extracted from blood plasma contained small quantities of FA as well.^{105–107} In the following decades, multiple binding sites were found for FA, and the binding affinity of fatty acid for HSA is mildly strong with an association constant in the range of 10^{-4} to 10^{-6} M^{-1} .^{108–112} As fatty acids are commercially inexpensive and can be readily attached to other pharmaceutical moieties, conjugating FA onto GLP (glucagon-like peptide) or insulin has been an effective way to develop long-acting antidiabetic therapeutics. For example, GLP-1 analog exendin-4 has been modified by two fatty acids: lauric acid (LUA, C12) and palmitic acid (PAA, C16) at its two lysine residues. The resulting FA-exendin-4 conjugates were tested as regulators of

blood glucose to cure type 2 diabetes, and showed a notably longer blood circulation profile over extendin-4 (Table 4).¹¹³ Additionally, the FA acylated insulin has also been developed as a long-circulating anti-diabetic drug. It binds at the long-chain fatty acid binding sites, but the binding affinity is lower than that of the free fatty acids and depends to a relatively small degree on the number of carbon atoms in the fatty acid. This FA insulin conjugate showed a prolonged circulatory half-life,¹¹⁴ but FA modification is not applicable to a broad set of molecules because of its negative effect on solubility.

3. Medical applications based on HSA-conjugates or HSA-binding moieties

3.1. Blood pool imaging agents

3.1.1. The efficacy of MRI contrast agents is improved by HSA-binding—The interest in the investigation of the binding ability towards HSA of paramagnetic complexes based on Gd(III), the most used T_1 contrast agents, is driven by two main reasons. First, the pharmacokinetic and pharmacodynamic properties of a HSA-binding contrast agent can be essentially effected by HSA, as the contrast agent is usually administered intravenously while HSA is the most predominant protein in the blood.^{115–118} After binding, the blood clearance of the contrast agent will be slowed down, and consequently the blood half-life and intravascular retention, will be increased.^{119–122} Thus, HSA-binding has been primarily considered for the visualization of vascular structures and for detecting regions with abnormal vascular permeability. Also, HSA binding can significantly improve the efficacy of these agents because the water proton relaxation time is strongly dependent on the tumbling motion of the metal complex.^{123–127}

As described previously, the presence of hydrophobic moieties as well as hydrophilic negatively charged groups are the basic structural requirements for binding pocket 2 of HSA, most of the work in this field has been focused on the design of metal complexes matching such features.^{124,125}

Gadofosveset or MS-325 (trade name: Ablavar, (trisodium 2-(*R*)-[(4,4-diphenylcyclohexyl)phosphonoxymethyl]diethylene-triaminepentaacetatoaquo gadolinium)) is a clinically approved gadolinium (Gd) based blood-pool MRI contrast agent (Fig. 12A) as an aid in diagnosing aortoiliac occlusive disease in patients with known or suspected peripheral vascular disease (PVD) or abdominal aortic aneurysm (AAA).¹¹⁷ As a result of transient binding to HSA, gadofosveset has ten times the signal-enhancing power of existing contrast agents as well as prolonged retention in the blood (Fig. 12B and C). This enables rapid acquisition of high-resolution magnetic resonance angiography (MRA) using standard MRI machines. Moreover, HSA binding offers an additional benefit beyond localization in the blood pool. The contrast agent begins to spin much more slowly, at the rate albumin spins, causing a relaxivity gain that produces a substantially brighter signal than would be possible with freely circulating gadolinium (Table 4).^{117,126–128}

The extended blood half-life of gadofosveset also results in a longer time period for imaging, which allows the radiologist to perform multiple imaging experiments and to image under steady-state conditions (Fig. 12G as an example).^{58,133–135} In addition to imaging peripheral vascular disease and coronary artery disease (Fig. 12D and F), current

trials are being conducted to evaluate gadofosveset as an aid in diagnosing breast cancer and to identify myocardial perfusion defects with delayed high-resolution imaging.^{136–138}

Another promising case of developing HSA-binding MRI contrast agent, 428-D-Lys- β -Ala-DTPA-Gd (Fig. 13A), was contributed by the Neri group, which also targets binding site 2.¹⁰⁴ The dissociation constant of 428-D-Lys- β -Ala-DTPA-Gd to HSA was determined by ITC at 37 °C ($K_d = 3.3 \mu\text{M}$, Fig. 13B), while Gd-DTPA had negligible binding to HSA. Pharmacokinetic profiles were studied in mice by injecting DTPA and 428-D-Lys- β -Ala-DTPA complexed with ¹⁷⁷Lu, thus allowing quantification by gamma-counting. Similar to the situation encountered with the fluorescein derivatives, the plasma concentration of DTPA-¹⁷⁷Lu decreased rapidly and was no longer detectable at 60 min after injection, whereas 428-D-Lys- β -Ala-DTPA-¹⁷⁷Lu displayed a substantially slower biphasic pharmacokinetic profile (Fig. 13C; DTPA-¹⁷⁷Lu: $t_{1/2} = 8.6 \text{ min}$ vs. 428-D-Lys- β -Ala-DTPA-¹⁷⁷Lu: $t_{1/2} = 408 \text{ min}$). The rapid extravasation of DTPA-Gd in comparison to 428-D-Lys- β -Ala-DTPA-Gd was also observed by MRI procedures following intravenous injection of the contrast agents. MRI analysis of major blood vessels of the brain revealed a slower decrease of signal intensities in those injected with 428-D-Lys- β -Ala-DTPA-Gd (Fig. 13C–E).

3.1.2. Radiolabeled HSA as the blood pool imaging agents—Although many radiolabeled HSA derivatives have been developed as blood pool agents for radionuclide imaging,^{139–144} the true revolution came from the recent report of ¹⁸F-NEB (Fig. 14A, NOTA conjugated truncated Evans blue), of which the preparation has been described previously.⁹⁹ Within a few minutes after tracer injection, ¹⁸F-NEB reached the highest SUV value in the blood. Afterwards, a slow but steady clearance of the radioactivity was observed from the blood, due to the turnover of albumin from blood circulation and slight dissociation of ¹⁸F-NEB from albumin. As shown in Fig. 14, this *in vivo* labeling strategy can be applied to blood-pool imaging to evaluate the cardiac function under both physiologic and pathologic conditions (Fig. 14B–D). This method can also be used to evaluate vascular permeability in tumors, inflammatory diseases, and ischemic or infarcted lesions.

Soon after the establishment of ¹⁸F-NEB, a first-in-human study was successfully performed with ⁶⁸Ga-labeled NEB (Fig. 14A). After intravenous injection, majority of the radioactivity was retained in the blood circulation due to the stable interaction of ⁶⁸Ga-NEB with serum albumin (Fig. 14B). A dosimetry study confirmed the safety with acceptable absorbed doses by critical organs even with multiple injections for one patient.

Overall, as a blood pool imaging agent, the preliminary clinical studies of ⁶⁸Ga-NEB demonstrate the value of differentiating hepatic hemangioma from other benign or malignant focal hepatic lesions. In addition, NEB can be easily labeled with different positron emitters of various half-lives and demonstrates promising pharmacokinetics in humans, warranting further clinical applications of NEB-based PET tracers.

3.1.3. Labeled HSA for lymph node mapping—Besides being a blood pool imaging agent, radiolabeled or fluorophore attached HSA is often used to noninvasively identify the lymph nodes for cancer diagnosis or guiding surgery.^{145–147} For instance, ^{99m}Tc-HSA has

been successfully applied to map sentinel lymph nodes for identifying the patients with melanoma and regional nodal micrometastasis, and exhibits a statistically better concordance rate than the radiotracers without HSA-conjugation.^{148,149}

As another good example, ¹⁸F-NEB (Fig. 14A) has also been applied to accurately locate sentinel lymph nodes.¹⁰⁰ After local injection, both ¹⁸F-AIF-NEB and EB form complexes with endogenous albumin in the interstitial fluid and allow for visualizing the lymphatic system. Positron emission tomography (PET) and/or optical imaging of LNs was performed in three different animal models including a hind limb inflammation model, an orthotropic breast cancer model, and a metastatic breast cancer model (Fig. 15). In these three models, the LNs can be distinguished clearly by using the blue color and the fluorescence signal from EB as well as the PET signal from ¹⁸F-NEB, suggesting that this combination of ¹⁸F-NEB and EB is potentially useful for mapping sentinel LNs and provide intraoperative guidance for clinical diagnosis.

3.2. HSA as a regulating platform for managing the blood sugar level

One of the most important clinical applications of the HSA-binding strategy is to elongate the blood circulation of anti-diabetic drugs. Up to now, three HSA-binding anti-diabetic drugs have been approved by U.S. FDA, and at least ten more candidates are under clinical tests.^{150–154}

Glucagon-like peptide (GLP)-1 is a 30-amino acid peptide hormone secreted from gut endocrine cells in response to nutrient ingestion that promotes nutrient assimilation through regulation of gastrointestinal motility and islet hormone secretion.¹⁵⁵ Infusion of GLP-1 into normal or diabetic human subjects stimulates insulin and inhibits glucagon secretion, thereby indirectly modulating peripheral glucose uptake and control of hepatic glucose production, therefore can enhance GLP-1 action for the treatment of type 2 diabetes.¹⁵⁶

A major challenge for the therapeutic use of regulatory peptides, including native GLP-1, is a short circulating $t_{1/2}$, due principally to rapid enzymatic inactivation and/or renal clearance. Although infusion of native GLP-1 is highly effective in lowering blood glucose in subjects with type 2 diabetes, a single subcutaneous injection of the native peptide is quickly degraded and disappears from the circulation within minutes.¹⁵⁷ Hence, the majority of pharmaceutical approaches to the development of GLP-1 mimetic agents have focused on the development of long-acting degradation-resistant peptides, such as Albugon, monoExendin-4 HSA (E1HSA), bisExendin-4 HSA (E2HSA), and so on. The pharmaceutical characteristics and pharmacokinetic properties of these HSA-binding or HSA containing anti-diabetic drugs are summarized in Table 5.

Albugon, or E1HSA, is a recombinant exendin-4-human serum albumin (HSA) fusion protein which retains the GLP-1 receptor binding activity of exendin-4 and as such is expected to exert glucose lowering effects with a prolonged duration (Fig. 16A).¹⁵⁸ In order to effectively bind to the GLP-1 receptor, HSA was fused at the C-terminus of Ex4 and a 5-aa linker (GGGGS) was inserted between them.¹⁵⁹ To determine the *in vivo* bioactivity of E1HSA, an oral glucose tolerance test (OGTT) was performed in diabetic db/db mice by a single injection of E1HSA. As shown in Fig. 16B–D, glucose tolerance in diabetic db/db

mice was effectively improved by EIHSA over the control group. In addition, an obvious dose-effect relationship was observed between the postdose serum glucose concentration and injection dose. Moreover, postdose time-course observation indicated that the glucose-lowering effect of EIHSA lasted for at least 24 hours.⁵⁷

3.3. HSA as a carrier for precision cancer therapy

HSA has long been a versatile drug carrier for developing effective anti-cancer agents. Upon binding to HSA, both the pharmaco-kinetics and pharmaceutical profiles of chemotherapeutic drugs may be changed to give better drug delivery efficiency as well as a less side effect. In this section, we summarize some of the recent developments in the field of HSA–drug conjugates, with the focus on chemotherapy and radiotherapy for cancers.

3.3.1. Albumin-bound drug nanoparticle increases the therapeutic index of conventional chemotherapy drugs

—In general, paclitaxel and other chemotherapeutic drugs are hydrophobic and thereby have poor solubility in blood circulation (Fig. 17A).^{2,164} To solve the problem, organic agents including polyethylated castor oil (Cremophor[®] EL) and ethanol are required in their clinical formulations as their vehicles.^{165,166} Nevertheless, these vehicles often cause severe toxicities, requiring prolonged infusion or premedication to reduce the risk of hypersensitivity reaction. Interestingly, albumin binds to many types of hydrophobic molecules in a reversible manner and consequently can help to transport the drugs in the body.^{10,167} Moreover, as an intrinsic protein carrier in the blood, utilizing albumin as the drug vehicle avoids the risk of hypersensitivity reaction caused by the artificial formulation, is thus capable of serving as a clinically safer platform to deliver hydrophobic drugs in the body.

Besides the reduced toxicity and less immunogenicity, albumin also assists the transportation of plasma constituents through endothelial cells *via* albumin receptor binding. Traditionally, only the unbound drugs were thought to be able to penetrate the vascular wall *via* junctional gaps between endothelial cells.¹⁶⁸ Nonetheless, a selective transportation mechanism was disclosed recently that albumin-bound molecules can cross vascular endothelium through albumin transcytosis.^{169–171} This process, illustrated in Fig. 17D, is thought to play a key role in delivering proteins across the vascular endothelium in order to meet the nutritional needs of cells. Because of its abnormal requirement of nutrition, tumors often take a higher level of albumin than healthy tissues, and thereby albumin-bound drugs can be delivered to tumor with better selectivity.

SPARC, which is short for the secreted protein that is acidic and rich in cysteine, is an extracellular matrix glycoprotein that is essentially related to tumor metastasis. It has been shown to be overexpressed on cancer cells and associated with poor prognosis in a number of tumors.¹⁷² Interestingly, recent evidence suggests that albumin exhibits high binding affinity to SPARC,^{173–176} and the tumor secretion of SPARC also plays a key role for the high tumor uptake of albumin.^{177,178} Therefore, the SPARC-inducing effect accumulates albumin to the areas of tumor that may further improve the delivery efficiency for albumin bound drugs (Fig. 17B and C).

Small molecular drug loaded albumin nanoparticles can be prepared in a number of ways, namely, desolvation,^{179,180} emulsification,^{181,182} thermal gelation,¹⁸³ nanospray drying,¹⁸⁴ nab-technology,¹⁶³ and self-assembly.¹⁸⁵ Here, we will mainly focus on nabTM-Technology, which is a biologically interactive delivery system that uses the biochemical properties of albumin to increase drug delivery to tumors. The first commercial product using this technology, Abraxane (*nab*-paclitaxel), is a solvent-free, 130 nm albumin particle form of paclitaxel. An *in vitro* experiment conducted by human lung microvessel endothelial cells indicated that the transportation of fluorescently labelled paclitaxel is about 4.2-fold greater rate across an endothelial cell monolayer when formulated as *nab*-paclitaxel than CrEL-paclitaxel (CrEL: Cremophor[®]EL, polyethylated castor oil). Because of its comparatively better efficacy for cancer treatment, Abraxane was approved by FDA in 2005 for the treatment of breast cancer cases where cancer did not respond to other chemotherapy (Fig. 18). In 2012 and 2013, Abraxane received approval from FDA to be used for the treatment of non-small cell lung cancer (NSCLC) as well as advanced prostate cancer because of its less toxicity during the treatment.

3.3.2. HSA–nanoparticle (NP) complex as a theranostic platform for diagnostic imaging and small molecular drug delivery—

In the past decade, the HSA–NP complex has been developed as a common nanoplatform with both imaging and therapeutic functions, denoted as “nanotheranostics”.^{2,26–28,85–90} For instance, after coupling with targeting ligands and imaging moieties, iron oxide nano-particles (IONPs) can provide many potential applications including multimodality imaging and therapy. In addition, HSA coated nanoparticles generally give reduced accumulation in mononuclear phagocytic system-related organs over the naked nanoparticles.^{85,87–91,186} In a pilot study, doxorubicin (Dox) was encapsulated into the HINPs (HSA coated iron oxide nanoparticles). About 0.5 mg of Dox and 1 mg of IONPs (iron oxide nanoparticles) could be loaded based on 10 mg of HSA matrices. The resulting D-HINPs (Dox loaded HINPs) could release Dox in a sustained fashion and effectively suppressed tumor growth that was much better than free Dox on a 4T1 murine breast cancer xenograft model.¹⁸⁶

This strategy was then extended to load other types of small molecules and to build a multimodal-imaging platform (Fig. 19). This combinational MRI/PET/NIRF theranostics nanosystem is capable of integrating the strengths of high anatomical resolution (MRI), *in vitro* validation (NIRF), quantitative evaluation (PET) and cancer treatment, and therefore can be a platform technology in theranostics.^{27,89–91,187}

3.3.3. Small molecule HSA conjugates for cancer chemotherapy—

The first HSA–drug conjugate that was evaluated in clinical trials was a HSA-conjugated chemotherapeutic drug: methotrexate–HSA conjugate (MTX–HSA). A phase I study with 17 patients treated with weekly MTX–HSA⁷⁷ found that two patients with renal cell carcinoma and one patient with mesothelioma responded to MTX–HSA therapy (one partial response, two minor responses). However, the clinical trial stopped at phase II as no objective response was seen with metastatic renal carcinoma.⁷⁸ The failure was most likely attributed to the drawbacks of MTX–HSA, such as the unclear chemical structure and unclear metabolic pathway of MTX–HSA.

By taking advantage of the *in vivo* maleimide–HSA conjugation strategy which was detailed in Section 2.2, DOXO-EMCH was highly effective in preclinical tumor models (Fig. 20). As expected, there was a pronounced difference between the levels of DOXO-EMCH and doxorubicin in the serum of MDA-MB-435 tumor mice. A good antitumor effect was achieved at $3 \times 16 \text{ mg kg}^{-1}$ doxorubicin equivalents and complete remission was found at $3 \times 24 \text{ mg kg}^{-1}$. Notably, preliminary toxicity studies in nude mice showed that the maximum tolerated dose of DOXO-EMCH was approximately 4.5 times higher than that of free doxorubicin.¹⁸⁸

DOXO-EMCH entered clinical trial in 2007, and was renamed INNO-206 or Aldoxorubicin in 2008. The on-going clinical studies suggest that INNO-206 can be administered safely at higher doses in patients than free doxorubicin, resulting in better efficacy compared with the currently available anthracyclines to treat several types of cancer.^{188,190,191}

3.3.4. Radiolabeled HSA-conjugate for internal radiotherapy of cancer—

In 2013, Shibili and his colleagues from ETH reported a strategy in which a DOTA–folate conjugate was coupled with a small molecule albumin binder, denoted as cm09. Radiolabeled folic acid derivatives have been used for folate receptor (FR) targeted imaging and therapy.^{192–194} However, using folate-based radiopharmaceuticals for therapy has long been regarded as an unattainable goal because of the poor tumor-to-kidney uptake ratio. As known, the rapid clearance of DOTA–folate conjugates from the blood circulation is generally considered as an advantage over the other targeting strategies.^{195–197} It is because rapid clearance usually gives high tumor-to-background contrast and therefore minimizes the exposure of major organs to the therapeutic probe.^{198–204} However, this pharmacokinetics is a double-bladed sword that is also responsible for the relatively low uptake of folate conjugates in tumor tissue and an extremely high accumulation of radioactivity in the kidneys.^{205–209} In addition, once the folate conjugate is cleared from blood into the renal system, most of them would be strongly trapped by the folate-binding protein in the kidneys, and therefore the kidney uptake of folate will not decrease over time.²⁰⁹ To solve this problem, this group reasoned that a HSA-binding radiopharmaceutical could change this dissatisfying situation as prolonged blood circulation could improve the tumor uptake, and reduce the problematic renal accumulation of the DOTA–folate conjugates.^{182,183}

As shown in Fig. 21, installation of an albumin-binding entity into the structure of a folate-based radioconjugate improved the overall tissue distribution significantly. Tumor uptake was doubled, and kidney retention was reduced to 30% of the value obtained with folate conjugates without an albumin-binding entity. In addition, tumor growth inhibition was observed without radiotoxic side effects.¹⁰³

4. Conclusions and outlook

As the key circulating protein in the blood circulation, albumin has been an excellent delivery platform for a number of endogenous and exogenous compounds. It has also been used to extend blood half-life and reduce renal clearance of both imaging probes and therapeutic drugs.

An ideal albumin-binding imaging probe may not only have a slow clearance from the blood, but also truly reflect a clear biological pathway in the body, *viz.*, the signal it provides needs to be correlated with circulation, metabolism and bioactivity of natural albumin. To accomplish this goal, the labeled albumin should be indistinguishable with natural albumin for *in vivo* bioactivity, and thus the imaging tag should be small in size, free of charge and stable *in vivo*. In addition, detachment of imaging reporters from the imaging probe should be avoided as it often gives misleading information for clinical diagnosis, and therefore the binding strategy to HSA has to be robust, covalent and irreversible, though some of the non-covalent binding strategies (*e.g.* Evans blue NOTA derivatives) also give promising results in the clinic. In addition, considering the clinical practice and operational simplicity, the HSA-binding imaging probe would better be a small molecule with unambiguous definition of chemistry; consequently the *in vivo* targeting strategy will be one of the choices for the future development of HSA-binding imaging probes.

In addition, in order to develop a more convenient and possibly less expensive treatment for diabetes, a HSA-binding blood glucose regulator would ideally have the longest if possible glucose-lowering effect without an apparent side effect to the patients. Meanwhile, to design a better HSA binding cancer therapeutic drug, the key here is to improve the tumor specificity, meaning increasing the tumor uptake while reducing the unnecessary cytotoxicity on healthy tissues. If possible, on-site drug release would be preferred, as it may essentially reduce the side effect since lower therapeutic dose would be applied to the patients.

In conclusion, as *in vitro* HSA conjugation chemistry has been well established, it is believed that the future of HSA-binding chemistry should focus on developing new *in vivo* HSA binders, either covalent or non-covalent. In addition, when a functional moiety is covalently coupled to HSA, the nonspecific adsorption of small molecules onto HSA is hard to be removed or purified, which is always a concern but can be avoided by *in vivo* targeting approaches. In the case of *in vivo* covalent binding, a faster and more bio-orthogonal conjugation method is in great need to improve the efficiency and selectivity of the binding reaction. For *in vivo* non-covalent binders, systematic chemical screening is necessary to develop a series of HSA binders toward different binding sites with various binding affinities. It is noteworthy that the strongest binder is not always in favor, as we may need a balance between blood retention and clearance in certain circumstances. Moreover, the space linker between the HSA-binding moiety and the functional molecule also needs more comprehensive investigation, and the ultimate goal would be a linker design that does not compromise the function of the albumin binder as well as the molecules of interest.

References

1. Kramer PA. J Pharm Sci. 1974; 63:1646–1647. [PubMed: 4436811]
2. Cho K, Wang X, Nie S, Chen Z, Shin DM. Clin Cancer Res. 2008; 14:1310–1316. [PubMed: 18316549]
3. Wunder A, Muller-Ladner U, Stelzer E, Neumann E, Sinn H, Gay S, Fiehn C. Arthritis Res Ther. 2003; 170:4793–4801.
4. Kratz F. J Controlled Release. 2008; 132:171–183.

5. Koehler MFT, Zobel K, Beresini MH, Caris LD, Combs D, Paasch BD, Lazarus RA. *Bioorg Med Chem Lett.* 2002; 12:2883–2886. [PubMed: 12270169]
6. Putnam, FW. *All About Albumin*. Peters, T., editor. Academic Press; San Diego: 1995. p. xi-xiii.
7. Sleep D, Cameron J, Evans LR. *Biochim Biophys Acta.* 2013; 1830:5526–5534. [PubMed: 23639804]
8. Anderson CL, Chaudhury C, Kim J, Bronson CL, Wani MA, Mohanty S. *Trends Immunol.* 2006; 27:343–348. [PubMed: 16731041]
9. Kim J, Hayton WL, Robinson JM, Anderson CL. *Clin Immunol.* 2007; 122:146–155. [PubMed: 17046328]
10. Elzoghby AO, Samy WM, Elgindy NA. *J Controlled Release.* 2012; 157:168–182.
11. Neumann E, Frei E, Funk D, Becker MD, Schrenk H-H, Müller-Ladner U, Fiehn C. *Expert Opin Drug Delivery.* 2010; 7:915–925.
12. Verrecchia T, Spenlehauer G, Bazile DV, Murry-Brelrier A, Archimbaud Y, Veillard M. *J Controlled Release.* 1995; 36:49–61.
13. Lu W, Zhang Y, Tan Y-Z, Hu K-L, Jiang X-G, Fu S-K. *J Controlled Release.* 2005; 107:428–448.
14. Baron MH, Baltimore D. *Cell.* 1982; 28:395–404. [PubMed: 6174242]
15. Bansal R, Prakash J, Ruijter Md, Beljaars L, Poelstra K. *Mol Pharmaceutics.* 2011; 8:1899–1909.
16. Ambros V, Baltimore D. *J Biol Chem.* 1978; 253:5263–5266. [PubMed: 209034]
17. Schilling U, Friedrich EA, Sinn H, Schrenk HH, Clorius JH, Maier-Borst W. *Int J Radiat Appl Instrum, Part B.* 1992; 19:685–695.
18. Tilton RD, Robertson CR, Gast AP. *J Colloid Interface Sci.* 1990; 137:192–203.
19. Lenkei R, Onica D, Ghetie V. *Experientia.* 1977; 33:1046–1047. [PubMed: 408179]
20. Elsadek B, Kratz F. *J Controlled Release.* 2012; 157:4–28.
21. Sleep D. *Expert Opin Drug Delivery.* 2014; 12:793–812.
22. Heneweer C, Holland JP, Divilov V, Carlin S, Lewis JS. *J Nucl Med.* 2011; 52:625–633. [PubMed: 21421727]
23. Cavalu S, Damian G, Dânsoreanu M. *Biophys Chem.* 2002; 99:181–188. [PubMed: 12377368]
24. Wunder A, Müller-Ladner U, Stelzer EHK, Funk J, Neumann E, Stehle G, Pap T, Sinn H, Gay S, Fiehn C. *J Immunol.* 2003; 170:4793–4801. [PubMed: 12707361]
25. Bolling C, Graefe T, Lübbling C, Jankevicius F, Uktveris S, Cesas A, Meyer-Moldenhauer WH, Starkmann H, Weigel M, Burk K, Hanauske AR. *Invest New Drugs.* 2006; 24:521–527. [PubMed: 16699974]
26. Wang W, Huang Y, Zhao S, Shao T, Cheng Y. *Chem Commun.* 2013; 49:2234–2236.
27. Zhao S, Wang W, Huang Y, Fu Y, Cheng Y. *MedChemComm.* 2014; 5:1658–1663.
28. Mier W, Hoffend J, Krämer S, Schuhmacher J, Hull WE, Eisenhut M, Haberkorn U. *Bioconjugate Chem.* 2005; 16:237–240.
29. Spanoghe M, Lanens D, Dommissie R, Van der Linden A, Alderweireldt F. *Magn Reson Imaging.* 1992; 10:913–917. [PubMed: 1334186]
30. Aldini R, Roda A, Labate AM, Cappelleri G, Roda E, Barbara L. *J Lipid Res.* 1982; 23:1167–1173. [PubMed: 7175373]
31. Hettick JM, Siegel PD, Green BJ, Liu J, Wisnewski AV. *Anal Biochem.* 2012; 421:706–711. [PubMed: 22206939]
32. Wong K, Cleland LG, Poznansky MJ. *Agents Actions.* 1980; 10:231–239. [PubMed: 7405750]
33. Shen WC, Ryser HJ. *Proc Natl Acad Sci U S A.* 1978; 75:1872–1876. [PubMed: 273916]
34. Lau S, Graham B, Cao N, Boyd BJ, Pouton CW, White PJ. *Mol Pharmaceutics.* 2012; 9:71–80.
35. McMenamy RH, Madeja MI, Watson F. *J Biol Chem.* 1968; 243:2328–2336. [PubMed: 4967583]
36. Choi JY, Jeong JM, Yoo BC, Kim K, Kim Y, Yang BY, Lee Y-S, Lee DS, Chung J-K, Lee MC. *Nucl Med Biol.* 2011; 38:371–379. [PubMed: 21492786]
37. Zhang YZ, Wang X, Feng Y, Li J, Lim CT, Ramakrishna S. *Biomacromolecules.* 2006; 7:1049–1057. [PubMed: 16602720]
38. Håkansson L, Venge PER. *APMIS.* 1994; 102:308–316. [PubMed: 8011308]

39. Hopf U, Büschenfelde K-HMz, Dierich MP. *J Immunol*. 1976; 117:639–645. [PubMed: 781134]
40. Mansour AM, Dreves J, Esser N, Hamada FM, Badary OA, Unger C, Fichtner I, Kratz F. *Cancer Res*. 2003; 63:4062–4066. [PubMed: 12874007]
41. Becker JM, Wilchek M, Katchalski E. *Proc Natl Acad Sci U S A*. 1971; 68:2604–2607. [PubMed: 4944635]
42. Kasina S, Rao TN, Srinivasan A, Sanderson JA, Fitzner JN, Reno JM, Beaumier PL, Fritzbeg AR. *J Nucl Med*. 1991; 32:1445–1451. [PubMed: 2066805]
43. Even GA, Green MA. *Int J Radiat Appl Instrum, Part B*. 1989; 16:319–321.
44. Chang YS, Jeong JM, Lee Y-S, Kim HW, Rai GB, Lee SJ, Lee DS, Chung J-K, Lee MC. *Bioconjugate Chem*. 2005; 16:1329–1333.
45. Wu S-Y, Kuo J-W, Chang T-K, Liu R-S, Lee R-C, Wang S-J, Lin W-J, Wang H-E. *Nucl Med Biol*. 2012; 39:1026–1033. [PubMed: 22762865]
46. Liu ZB, Li Y, Lozada J, Schaffer P, Adam MJ, Ruth TJ, Perrin DM. *Angew Chem, Int Ed*. 2013; 52:2303–2307.
47. Liu Z, Chen H, Chen K, Shao Y, Kiesewetter DO, Niu G, Chen X. *Sci Adv*. 2015; 1:e1500694. [PubMed: 26601275]
48. Šimeček J, Notni J, Kapp TG, Kessler H, Wester H-J. *Mol Pharmaceutics*. 2014; 11:1687–1695.
49. Bernard-Gauthier V, Bailey JJ, Liu Z, Wängler B, Wängler C, Jurkschat K, Perrin DM, Schirmacher R. *Bioconjugate Chem*. 2015; doi: 10.1021/acs.bioconjchem.5b00560
50. Liu Z, Li Y, Lozada J, Wong MQ, Greene J, Lin K-S, Yapp D, Perrin DM. *Nucl Med Biol*. 2013; 40:841–849. [PubMed: 23810487]
51. Palmowski M, Goedicke A, Vogg A, Christ G, Mühlenbruch G, Kaiser H, Günther R, Kuhl C, Mottaghy F, Behrendt F. *Eur Radiol*. 2013; 23:3062–3070. [PubMed: 23771601]
52. Ogan MD, Schmiedl U, Moseley ME, Grodd W, Paaajanen H, Brasch RC. *Invest Radiol*. 1987; 22:665–671. [PubMed: 3667174]
53. Todica A, Brunner S, Böning G, Lehner S, Nekolla S, Wildgruber M, Übleis C, Wängler C, Sauter M, Klingel K, Cumming P, Bartenstein P, Schirmacher R, Franz W, Hacker M. *Mol Imaging Biol*. 2013; 15:441–449. [PubMed: 23408338]
54. Kratz F, Dreves J, Bing G, Stockmar C, Scheuermann K, Lazar P, Unger C. *Bioorg Med Chem Lett*. 2001; 11:2001–2006. [PubMed: 11454467]
55. Rong P, Huang P, Liu Z, Lin J, Jin A, Ma Y, Niu G, Yu L, Zeng W, Wang W, Chen X. *Nanoscale*. 2015; 7:16330–16336. [PubMed: 26382146]
56. Burke CW, Shakespear RA. *J Endocrinol*. 1975; 65:133–138. [PubMed: 1141804]
57. Zhang L, Wang L, Meng Z, Gan H, Gu R, Wu Z, Gao L, Zhu X, Sun W, Li J, Zheng Y, Dou G. *Biochem Biophys Res Commun*. 2014; 445:511–516. [PubMed: 24565847]
58. Liu X, Bi X, Huang J, Jerecic R, Carr J, Li D. *Invest Radiol*. 2008; 43:663–668. [PubMed: 18708861]
59. Melder R, Osborn B, Riccobene T, Kanakaraj P, Wei P, Chen G, Stalow D, Halpern W, Migone T-S, Wang Q, Grzegorzewski K, Gallant G. *Cancer Immunol Immunother*. 2005; 54:535–547. [PubMed: 15592670]
60. Kratz F, Müller-Driver R, Hofmann I, Dreves J, Unger C. *J Med Chem*. 2000; 43:1253–1256. [PubMed: 10753462]
61. Etoh T, Miyazaki M, Harada K, Nakayama M, Sugii A. *J Chromatogr B: Biomed Sci Appl*. 1992; 578:292–296.
62. Era S, Hamaguchi T, Sogami M, Kuwata K, Suzuki E, Miura K, Kawai K, Kitazawa Y, Okabe H, Noma A, Miyata S. *Int J Pept Protein Res*. 1988; 31:435–442. [PubMed: 3410634]
63. Coleman RD, Kim TW, Gotto AM Jr, Yang C-y. *Biochim Biophys Acta*. 1990; 1037:129–132. [PubMed: 2294968]
64. Ferguson E, Singh RJ, Hogg N, Kalyanaraman B. *Arch Biochem Biophys*. 1997; 341:287–294. [PubMed: 9169017]
65. Yang CY, Kim TW, Weng SA, Lee BR, Yang ML, Gotto AM. *Proc Natl Acad Sci U S A*. 1990; 87:5523–5527. [PubMed: 2115173]

66. Smith DE, Mosher DF, Johnson RB, Furcht LT. *J Biol Chem.* 1982; 257:5831–5838. [PubMed: 6175633]
67. Larsson LJ, Lindahl P, Hallén-Sandgren C, Björk I. *Biochem J.* 1987; 243:47–54. [PubMed: 2440424]
68. Zissimopoulos S, Marsh J, Stannard L, Seidel M, Lai FA. *Biochem J.* 2014; 459:265–273. [PubMed: 24502647]
69. Kratz F, Warnecke A, Scheuermann K, Stockmar C, Schwab J, Lazar P, Drückes P, Esser N, Drevs J, Rognan D, Bissantz C, Hinderling C, Folkers G, Fichtner I, Unger C. *J Med Chem.* 2002; 45:5523–5533. [PubMed: 12459020]
70. Schmid B, Chung D-E, Warnecke A, Fichtner I, Kratz F. *Bioconjugate Chem.* 2007; 18:702–716.
71. Chung D-E, Kratz F. *Bioorg Med Chem Lett.* 2006; 16:5157–5163. [PubMed: 16875815]
72. Kratz F, Mansour A, Soltau J, Warnecke A, Fichtner I, Unger C, Drevs J. *Arch Pharm.* 2005; 338:462–472.
73. Warnecke A, Fichtner I, Saß G, Kratz F. *Arch Pharm.* 2007; 340:389–395.
74. Schmid B, Warnecke A, Fichtner I, Jung M, Kratz F. *Bioconjugate Chem.* 2007; 18:1786–1799.
75. Warnecke A, Fichtner I, Garmann D, Jaehde U, Kratz F. *Bioconjugate Chem.* 2004; 15:1349–1359.
76. Abu Ajaj K, Graeser R, Fichtner I, Kratz F. *Cancer Chemother Pharmacol.* 2009; 64:413–418. [PubMed: 19229536]
77. Hartung G, Stehle G, Sinn H, Wunder A, Schrenk HH, Heeger S, Kränzle M, Edler L, Frei E, Fiebig HH, Heene DL, Maier-Borst W, Queisser W. *Clin Cancer Res.* 1999; 5:753–759. [PubMed: 10213209]
78. Vis A, van der Gaast A, van Rhijn B, Catsburg T, Schmidt C, Mickisch G. *Cancer Chemother Pharmacol.* 2002; 49:342–345. [PubMed: 11914915]
79. Ross PD, Subramanian S. *Biochemistry.* 1981; 20:3096–3102. [PubMed: 7248271]
80. Grymonpré KR, Staggemeier BA, Dubin PL, Mattison KW. *Biomacromolecules.* 2001; 2:422–429. [PubMed: 11749202]
81. Bledin AG, Kantarjian HM, Kim EE, Wallace S, Chuang VP, Patt YZ, Haynie TP. *Am J Roentgenol.* 1982; 139:711–715. [PubMed: 6214932]
82. Watanabe N, Shirakami Y, Tomiyoshi K, Oriuchi N, Hirano T, Higuchi T, Inoue T, Endo K. *J Nucl Med.* 1997; 38:1590–1592. [PubMed: 9379197]
83. Miskowiak J, Nielsen SL, Munck O. *Radiology.* 1981; 141:499–504. [PubMed: 6457317]
84. Zhao F, Shen G, Chen C, Xing R, Zou Q, Ma G, Yan X. *Chem – Eur J.* 2014; 20:6880–6887. [PubMed: 24828788]
85. Lee H-Y, Li Z, Chen K, Hsu AR, Xu C, Xie J, Sun S, Chen X. *J Nucl Med.* 2008; 49:1371–1379. [PubMed: 18632815]
86. Swierczewska M, Lee S, Chen X. *Mol Imaging.* 2011; 10:3–16. [PubMed: 21303611]
87. Quan Q, Xie J, Gao H, Yang M, Zhang F, Liu G, Lin X, Wang A, Eden HS, Lee S, Zhang G, Chen X. *Mol Pharmaceutics.* 2011; 8:1669–1676.
88. Gao J, Chen K, Xie R, Xie J, Lee S, Cheng Z, Peng X, Chen X. *Small.* 2010; 6:256–261. [PubMed: 19911392]
89. Huang J, Bu L, Xie J, Chen K, Cheng Z, Li X, Chen X. *ACS Nano.* 2010; 4:7151–7160. [PubMed: 21043459]
90. Xie J, Liu G, Eden HS, Ai H, Chen X. *Acc Chem Res.* 2011; 44:883–892. [PubMed: 21548618]
91. Xie J, Chen K, Huang J, Lee S, Wang J, Gao J, Li X, Chen X. *Biomaterials.* 2010; 31:3016–3022. [PubMed: 20092887]
92. He XM, Carter DC. *Nature.* 1992; 358:209–215. [PubMed: 1630489]
93. Ghuman J, Zunszain PA, Petipras I, Bhattacharya AA, Otagiri M, Curry S. *J Mol Biol.* 2005; 353:38–52. [PubMed: 16169013]
94. Sudlow G, Birkett DJ, Wade DN. *Mol Pharmacol.* 1975; 11:824–832. [PubMed: 1207674]
95. Dockal M, Carter DC, Rüker F. *J Biol Chem.* 1999; 274:29303–29310. [PubMed: 10506189]
96. Peters, T, Jr. *All About Albumin.* Peters, T., editor. Academic Press; San Diego: 1995. p. 76-132.
97. Wanwimolruk S, Birkett DJ, Brooks PM. *Mol Pharmacol.* 1983; 24:458–463. [PubMed: 6195516]

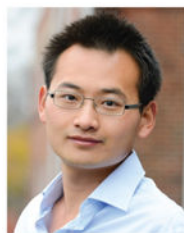
98. Crooke AC, Morris CJO. *J Physiol.* 1942; 101:217–223. [PubMed: 16991555]
99. Niu G, Lang L, Kiesewetter DO, Ma Y, Sun Z, Guo N, Guo J, Wu C, Chen X. *J Nucl Med.* 2014; 55:1150–1156. [PubMed: 24842890]
100. Wang Y, Lang L, Huang P, Wang Z, Jacobson O, Kiesewetter DO, Ali IU, Teng G, Niu G, Chen X. *Proc Natl Acad Sci U S A.* 2015; 112:208–213. [PubMed: 25535368]
101. Zhang J, Lang L, Zhu Z, Li F, Niu G, Chen X. *J Nucl Med.* 2015; 56:1609–1614. [PubMed: 26251416]
102. Skowronek M, Roterman I, Konieczny L, Stopa B, Rybarska J, Piekarska B. *J Comput Chem.* 2000; 21:656–667.
103. Müller C, Schibli R. *Front Oncol.* 2013; 3:249. [PubMed: 24069581]
104. Dumelin CE, Trüssel S, Buller F, Trachsel E, Bootz F, Zhang Y, Mannocci L, Beck SC, Drumea-Mirancea M, Seeliger MW, Baltés C, Müggler T, Kranz F, Rudin M, Melkko S, Scheuermann J, Neri D. *Angew Chem, Int Ed.* 2008; 47:3196–3201.
105. Goodman DS. *J Am Chem Soc.* 1958; 80:3892–3898.
106. Chen RF. *J Biol Chem.* 1967; 242:173–181. [PubMed: 6016603]
107. Spector AA. *J Lipid Res.* 1975; 16:165–179. [PubMed: 236351]
108. van der Vusse GJ. *Drug Metab Pharmacokinet.* 2009; 24:300–307. [PubMed: 19745557]
109. Alvarez JG, Storey BT. *Mol Reprod Dev.* 1995; 42:334–346. [PubMed: 8579848]
110. Richieri GV, Anel A, Kleinfeld AM. *Biochemistry.* 1993; 32:7574–7580. [PubMed: 8338853]
111. Curry S, Brick P, Franks NP. *Biochim Biophys Acta.* 1999; 1441:131–140. [PubMed: 10570241]
112. Fletcher JE, Spector AA, Ashbrook JD. *Biochemistry.* 1971; 10:3229–3232. [PubMed: 5165844]
113. Chae SY, Choi YG, Son S, Jung SY, Lee DS, Lee KC. *J Controlled Release.* 2010; 144:10–16.
114. Kurtzhals P, Havelund S, Jonassen I, Kiehr B, Larsen UD, Ribøl U, Markussen J. *Biochem J.* 1995; 312:725–731. [PubMed: 8554512]
115. Nagaraja TN, Croxson RL, Panda S, Knight RA, Keenan KA, Brown SL, Fenstermacher JD, Ewing JR. *J Neurosci Methods.* 2006; 157:238–245. [PubMed: 16769125]
116. Schwitter J, Saeed M, Wendland MF, Derugin N, Canet E, Brasch RC, Higgins CB. *J Am Coll Cardiol.* 1997; 30:1086–1094. [PubMed: 9316544]
117. McMurry TJ, Parmelee DJ, Sajiki H, Scott DM, Ouellet HS, Walovitch RC, Tyeklár Z, Dumas S, Bernard P, Nadler S, Midelfort K, Greenfield M, Troughton J, Lauffer RB. *J Med Chem.* 2002; 45:3465–3474. [PubMed: 12139457]
118. Reuben J. *J Phys Chem.* 1971; 75:3164–3167.
119. McDonald MA, Watkin KL. *Invest Radiol.* 2003; 38:305–310. [PubMed: 12908697]
120. Aime S, Chiaussa M, Digilio G, Gianolio E, Terreno E. *JBIC, J Biol Inorg Chem.* 1999; 4:766–774. [PubMed: 10631608]
121. Caravan P, Parigi G, Chasse JM, Cloutier NJ, Ellison JJ, Lauffer RB, Luchinat C, McDermid SA, Spiller M, McMurry TJ. *Inorg Chem.* 2007; 46:6632–6639. [PubMed: 17625839]
122. Reuben J. *Biochemistry.* 1971; 10:2834–2838. [PubMed: 4329808]
123. Fasano M, Curry S, Terreno E, Galliano M, Fanali G, Narciso P, Notari S, Ascenzi P. *IUBMB Life.* 2005; 57:787–796. [PubMed: 16393781]
124. Prasad PV, Cannillo J, Chavez DR, Pinchasin ES, Dolan RP, Walovitch R, Edelman RR. *Invest Radiol.* 1999; 34:566. [PubMed: 10485071]
125. Krause MHJ, Kwong KK, Xiong J, Gragoudas ES, Young LHY. *Magn Reson Imaging.* 2003; 21:725–732. [PubMed: 14559336]
126. Rapp JH, Wolff SD, Quinn SF, Soto JA, Meranze SG, Muluk S, Blebea J, Johnson SP, Rofsky NM, Duerinckx A, Foster GS, Kent KC, Moneta G, Middlebrook MR, Narra VR, Toombs BD, Pollak J, Yucel EK, Shamsi K, Weisskoff RM. *Radiology.* 2005; 236:71–78. [PubMed: 15987963]
127. Caravan P, Cloutier NJ, Greenfield MT, McDermid SA, Dunham SU, Bulte JWM, Amedio JC, Looby RJ, Supkowski RM, Horrocks WD, McMurry TJ, Lauffer RB. *J Am Chem Soc.* 2002; 124:3152–3162. [PubMed: 11902904]

128. Zobel K, Koehler MFT, Beresini MH, Caris LD, Combs D. *Bioorg Med Chem Lett*. 2003; 13:1513–1515. [PubMed: 12699744]
129. Goyen M. *Vasc Health Risk Manage*. 2008; 4:1–9.
130. Raymond KN, Pierre VC. *Bioconjugate Chem*. 2005; 16:3–8.
131. Caravan P, Ellison JJ, McMurry TJ, Lauffer RB. *Chem Rev*. 1999; 99:2293–2352. [PubMed: 11749483]
132. Yang C-T, Chuang K-H. *MedChemComm*. 2012; 3:552–565.
133. Michaely HJ, Attenberger UI, Dietrich O, Schmitt P, Nael K, Kramer H, Reiser MF, Schoenberg SO, Walz M. *Invest Radiol*. 2008; 43:635–641. [PubMed: 18708857]
134. Haneder S, Attenberger UI, Biffar A, Dietrich O, Fink C, Schoenberg SO, Michaely HJ. *Invest Radiol*. 2011; 46:678–685. [PubMed: 21709565]
135. Anzidei M, Napoli A, Marincola BC, Kirchin MA, Neira C, Geiger D, Zaccagna F, Catalano C, Passariello R. *Invest Radiol*. 2009; 44:784–792. [PubMed: 19858728]
136. Schipper R-J, Smidt ML, van Roozendaal LM, Castro CJG, de Vries B, Heuts EM, Keymeulen KBMI, Wildberger JE, Lobbes MBI, Beets-Tan RGH. *Invest Radiol*. 2013; 48:134–139. [PubMed: 23262788]
137. Rahbar H, Partridge SC, Javid SH, Lehman CD. *Curr Probl Diagn Radiol*. 2012; 41:149–158. [PubMed: 22818835]
138. O’Flynn E, deSouza N. *Breast Cancer Res*. 2011; 13:204. [PubMed: 21392409]
139. Rogers DF, Boschetto P, Barnes PJ. *J Pharmacol Methods*. 1989; 21:309–315. [PubMed: 2755146]
140. Martínez-Palones JM, Gil-Moreno A, Pérez-Benavente MaA, Roca I, Xercavins J. *Gynecol Oncol*. 2004; 92:845–850. [PubMed: 14984951]
141. Patterson CE, Rhoades RA, Garcia JG. *J Appl Physiol*. 1992; 72:865–873. [PubMed: 1568982]
142. Verrecchia T, Huve P, Bazile D, Veillard M, Spenlehauer G, Couvreur P. *J Biomed Mater Res*. 1993; 27:1019–1028. [PubMed: 8408114]
143. Partridge WM, Eisenberg J, Cefalu WT. *Am J Physiol: Endocrinol Metab*. 1985; 249:E264–E267.
144. Desai NP, Hubbell JA. *J Biomed Mater Res*. 1991; 25:829–843. [PubMed: 1833405]
145. Bedrosian I, Scheff AM, Mick R, Callans LS, Bucky LP, Spitz FR, Helsabeck C, Elder DE, Alavi A, Fraker DF, Czerniecki BJ. *J Nucl Med*. 1999; 40:1143–1148. [PubMed: 10405134]
146. Albertini JJ, Lyman GH, Cox C, et al. *J Am Med Assoc*. 1996; 276:1818–1822.
147. Veronesi U, Paganelli G, Viale G, Galimberti V, Luini A, Zurrada S, Robertson C, Sacchini V, Veronesi P, Orvieto E, De Cicco C, Intra M, Tosi G, Scarpa D. *J Natl Cancer Inst*. 1999; 91:368–373. [PubMed: 10050871]
148. Maccauro M, Lucignani G, Aliberti G, Villano C, Castellani M, Solima E, Bombardieri E. *Eur J Nucl Med Mol Imaging*. 2005; 32:569–574. [PubMed: 15625604]
149. Wilhelm AJ, Mijnhout GS, Franssen EJF. *Eur J Nucl Med*. 1999; 26:S36–S42. [PubMed: 10199931]
150. Ahrén B, Schmitz O. *Horm Metab Res*. 2004; 36:867–876. [PubMed: 15655721]
151. Nauck MA, Vardarli I, Deacon CF, Holst JJ, Meier JJ. *Diabetologia*. 2011; 54:10–18. [PubMed: 20871975]
152. Baggio LL, Huang Q, Brown TJ, Drucker DJ. *Diabetes*. 2004; 53:2492–2500. [PubMed: 15331566]
153. Kim J-G, Baggio LL, Bridon DP, Castaigne J-P, Robitaille MF, Jetté L, Benquet C, Drucker DJ. *Diabetes*. 2003; 52:751–759. [PubMed: 12606517]
154. Meier JJ. *Nat Rev Endocrinol*. 2012; 8:728–742. [PubMed: 22945360]
155. Kreyman B, Ghatei MA, Williams G, Bloom SR. *Lancet*. 1987; 330:1300–1304.
156. Turton MD, O’Shea D, Gunn I, Beak SA, Edwards CMB, Meeran K, Choi SJ, Taylor GM, Heath MM, Lambert PD, Wilding JPH, Smith DM, Ghatei MA, Herbert J, Bloom SR. *Nature*. 1996; 379:69–72. [PubMed: 8538742]
157. Drucker DJ, Nauck MA. *Lancet*. 2006; 368:1696–1705. [PubMed: 17098089]

158. Hou S, Li C, Huan Y, Liu S, Liu Q, Sun S, Jiang Q, Jia C, Shen Z. *J Diabetes Res.* 2015; 2015:817839. [PubMed: 26351642]
159. Pollaro L, Heinis C. *MedChemComm.* 2010; 1:319–324.
160. Rosenstock J, Reusch J, Bush M, Yang F, Stewart M. G for the Albiglutide Study. *Diabetes Care.* 2009; 32:1880–1886. [PubMed: 19592625]
161. Rosenstock J, Reusch J, Bush M, Yang F, Stewart M. ftAS Group. *Diabetes Care.* 2009; 32:1880–1886. [PubMed: 19592625]
162. Cai Y, Yue P. *J Chromatogr A.* 2011; 1218:6953–6960. [PubMed: 21862025]
163. Cortes J, Saura C. *Eur J Cancer Suppl.* 2010; 8:1–10.
164. Gradishar WJ, Tjulandin S, Davidson N, Shaw H, Desai N, Bhar P, Hawkins M, O'Shaughnessy J. *J Clin Oncol.* 2005; 23:7794–7803. [PubMed: 16172456]
165. Lluch A, Álvarez I, Muñoz M, Á Seguí M, Tusquets I, García-Estévez L. *Crit Rev Oncol Hematol.* 2014; 89:62–72. [PubMed: 24071503]
166. Cucinotto I, Fiorillo L, Gualtieri S, Arbitrio M, Ciliberto D, Staropoli N, Grimaldi A, Luce A, Tassone P, Caraglia M, Tagliaferri P. *J Drug Delivery.* 2013; 2013:10.
167. Chen H, Huang X, Wang S, Zheng X, Lin J, Li P, Lin L. *Chin J Cancer Res.* 2015; 27:190–196. [PubMed: 25937781]
168. Dennis MS, Jin H, Dugger D, Yang R, McFarland L, Ogasawara A, Williams S, Cole MJ, Ross S, Schwall R. *Cancer Res.* 2007; 67:254–261. [PubMed: 17210705]
169. John TA, Vogel SM, Tirupathi C, Malik AB, Minshall RD. *Am J Physiol: Lung Cell Mol Physiol.* 2003; 284:L187–L196. [PubMed: 12471015]
170. Riehemann K, Schneider SW, Luger TA, Godin B, Ferrari M, Fuchs H. *Angew Chem, Int Ed.* 2009; 48:872–897.
171. Sahay G, Alakhova DY, Kabanov AV. *J Controlled Release.* 2010; 145:182–195.
172. Shi Q, Bao S, Song L, Wu Q, Bigner DD, Hjelmeland AB, Rich JN. *Oncogene.* 2007; 26:4084–4094. [PubMed: 17213807]
173. Neuzillet C, Tijeras-Raballand A, Cros J, Faivre S, Hammel P, Raymond E. *Cancer Metastasis Rev.* 2013; 32:585–602. [PubMed: 23690170]
174. Desai N, Trieu V, Damascelli B, Soon-Shiong P. *Transl Oncol.* 2009; 2:59–64. [PubMed: 19412420]
175. Haber CL, Gottifredi V, Llera AS, Salvatierra E, Prada F, Alonso L, Helene SE, Podhajcer OL. *Int J Cancer.* 2008; 122:1465–1475. [PubMed: 18059024]
176. Huang Y, Zhang J, Zhao Y-Y, Jiang W, Xue C, Xu F, Zhao H-Y, Zhang Y, Zhao L-P, Hu Z-H, Yao Z-W, Liu Q-Y, Zhang L. *Chin J Cancer.* 2012; 31:541–548. [PubMed: 23114088]
177. Schnitzer JE, Oh P. *Am J Physiol: Heart Circ Physiol.* 1992; 263:H1872–H1879.
178. Lane TF, Sage EH. *FASEB J.* 1994; 8:163–173. [PubMed: 8119487]
179. Vandelli MA, Rivasi F, Guerra P, Forni F, Arletti R. *Int J Pharm.* 2001; 215:175–184. [PubMed: 11250103]
180. Weber C, Coester C, Kreuter J, Langer K. *Int J Pharm.* 2000; 194:91–102. [PubMed: 10601688]
181. Crisante F, Francolini I, Bellusci M, Martinelli A, D'Ilario L, Piozzi A. *Eur J Pharm Sci.* 2009; 36:555–564. [PubMed: 19136061]
182. Yang L, Cui F, Cun D, Tao A, Shi K, Lin W. *Int J Pharm.* 2007; 340:163–172. [PubMed: 17482779]
183. Qi J, Yao P, He F, Yu C, Huang C. *Int J Pharm.* 2010; 393:177–185.
184. Lee SH, Heng D, Ng WK, Chan H-K, Tan RBH. *Int J Pharm.* 2011; 403:192–200. [PubMed: 20951781]
185. Gong J, Huo M, Zhou J, Zhang Y, Peng X, Yu D, Zhang H, Li J. *Int J Pharm.* 2009; 376:161–168. [PubMed: 19409461]
186. Xie J, Wang J, Niu G, Huang J, Chen K, Li X, Chen X. *Chem Commun.* 2010; 46:433–435.
187. Kirchner C, Liedl T, Kudera S, Pellegrino T, Muñoz Javier A, Gaub HE, Stölzle S, Fertig N, Parak WJ. *Nano Lett.* 2005; 5:331–338. [PubMed: 15794621]

188. Kratz F, Ehling G, Kauffmann H-M, Unger C. *Hum Exp Toxicol*. 2007; 26:19–35. [PubMed: 17334177]
189. Kratz F. *Expert Opin Invest Drugs*. 2007; 16:855–866.
190. Sanchez E, Li M, Wang C, Nichols CM, Li J, Chen H, Berenson JR. *Clin Cancer Res*. 2012; 18:3856–3867. [PubMed: 22619306]
191. Kratz F, Fichtner I, Graeser R. *Invest New Drugs*. 2012; 30:1743–1749. [PubMed: 21590366]
192. Sudimack J, Lee RJ. *Adv Drug Delivery Rev*. 2000; 41:147–162.
193. Wiener EC, Konda S, Shadron A, Brechbiel M, Gansow O. *Invest Radiol*. 1997; 32:748–754. [PubMed: 9406015]
194. Parker N, Turk MJ, Westrick E, Lewis JD, Low PS, Leamon CP. *Anal Biochem*. 2005; 338:284–293. [PubMed: 15745749]
195. Smith-Jones PM, Pandit-Taskar N, Cao W, O'Donoghue J, Philips MD, Carrasquillo J, Konner JA, Old LJ, Larson SM. *Nucl Med Biol*. 2008; 35:343–351. [PubMed: 18355690]
196. Müller C, Vlahov IR, Santhapuram HKR, Leamon CP, Schibli R. *Nucl Med Biol*. 2011; 38:715–723. [PubMed: 21718947]
197. Fani M, Wang X, Nicolas G, Medina C, Raynal I, Port M, Maecke H. *Eur J Nucl Med Mol Imaging*. 2011; 38:108–119. [PubMed: 20799032]
198. Liu Z, Amouroux G, Zhang Z, Pan J, Hundal-Jabal N, Colpo N, Lau J, Perrin DM, Bénard F, Lin K-S. *Mol Pharmaceutics*. 2015; 12:974–982.
199. Port M, Corot C, Rousseaux O, Raynal I, Devoldere L, Idée J-M, Dencausse A, Greneur S, Simonot C, Meyer D. *Magn Reson Mater Phys, Biol Med*. 2001; 12:121–127.
200. Kowalski J, Henze M, Schuhmacher J, Mäcke HR, Hofmann M, Haberkorn U. *Mol Imaging Biol*. 2003; 5:42–48. [PubMed: 14499161]
201. Liu Z, Pourghiasian M, Bénard F, Pan J, Lin K-S, Perrin DM. *J Nucl Med*. 2014; 55:1499–1505. [PubMed: 24970911]
202. Velikyan I, Sundberg ÅL, Lindhe Ö, Höglund AU, Eriksson O, Werner E, Carlsson J, Bergström M, Långström B, Tolmachev V. *J Nucl Med*. 2005; 46:1881–1888. [PubMed: 16269603]
203. Ugur Ö, Kothari PJ, Finn RD, Zanzonico P, Ruan S, Guenther I, Maecke HR, Larson SM. *Nucl Med Biol*. 2002; 29:147–157. [PubMed: 11823119]
204. Liu Z, Pourghiasian M, Radtke MA, Lau J, Pan J, Dias GM, Yapp D, Lin K-S, Bénard F, Perrin DM. *Angew Chem, Int Ed*. 2014; 53:11876–11880.
205. Selhub J, Franklin WA. *J Biol Chem*. 1984; 259:6601–6606. [PubMed: 6427219]
206. Selhub J, Emmanouel D, Stavropoulos T, Arnold R. *Am J Physiol: Renal, Fluid Electrolyte Physiol*. 1987; 252:F750–F756.
207. Birn H, Selhub J, Christensen EI. *Am J Physiol: Cell Physiol*. 1993; 264:C302–C310.
208. Weitman SD, Lark RH, Coney LR, Fort DW, Frasca V, Zurawski VR, Kamen BA. *Cancer Res*. 1992; 52:3396–3401. [PubMed: 1596899]
209. Hjelle JT, Christensen EI, Carone FA, Selhub J. *Am J Physiol: Cell Physiol*. 1991; 260:C338–C346.
210. Müller C, Struthers H, Winiger C, Zhernosekov K, Schibli R. *J Nucl Med*. 2013; 54:124–131. [PubMed: 23236020]
211. Kim TH, Park CW, Kim HY. *Biol Pharm Bull*. 2012; 35:1076–1083. [PubMed: 22791155]

Biographies



Zhibo Liu

Zhibo (Zippo) Liu received his BS in Chemistry from Nanjing University in 2010, and PhD in Chemistry from the University of British Columbia in 2014. Under the supervision of Drs David M. Perrin, Kuo-Shyan Lin, and François Bénard, he developed a broadly applicable one-step ^{18}F -labeling method based on a novel organo-trifluoroborate. Right after graduation, he joined the Laboratory of Molecular Imaging and Nanomedicine (LOMIN) at National Institutes of Health (NIH) as a postdoctoral research fellow under the supervision of Dr Xiaoyuan (Shawn) Chen. His research focuses on developing albumin-binding imaging probes as well as utilizing boramino acid to identify tumor from inflammation for early cancer diagnosis.



Xiaoyuan Chen

Xiaoyuan (Shawn) Chen received his PhD in chemistry from the University of Idaho in 1999. After being a faculty member at the University of Southern California and Stanford University, he joined the Intramural Research Program of the NIBIB in 2009 as a Senior Investigator and Chief of the Laboratory of Molecular Imaging and Nanomedicine (LOMIN). Dr Chen has published over 500 papers (H-index = 90) and numerous books and book chapters. He sits on the editorial board of over 10 peer-reviewed journals and is the founding editor of the journal *Theranostics*. His lab focuses on developing molecular imaging probes and nanotechnologies for early diagnosis of disease, monitoring therapy responses, and guiding drug discovery/development.

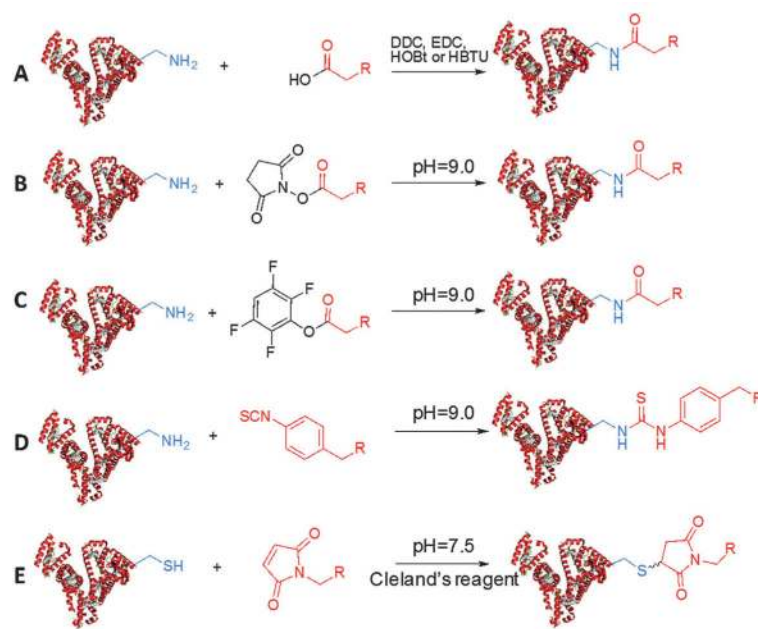


Fig. 1.

General methods of covalently conjugating small molecules onto albumin. (A) The coupling molecule is activated *in situ* by using classical coupling reagents such as *N,N'*-dicyclohexylcarbodiimide (DCC), 1-ethyl-3-(3-dimethylaminopropyl)carbodiimide (EDC), hydroxybenzotriazole (HOBT) and 2-(1*H*-benzotriazol-1-yl)-1,1,3,3-tetramethyluronium hexafluorophosphate (HBTU), and then attached onto lysine residue of HSA under weakly basic conditions. (B) The coupling molecule is activated as an *N*-hydroxysuccinimide (NHS) ester prior to be conjugated onto lysine residue of HSA under weakly basic conditions. (C) The coupling molecule is activated as a tetrafluorophenyl (TFP) ester prior to being conjugated onto lysine residue of HSA under weakly basic conditions. (D) The coupling molecule is modified to contain *p*-isothiocyanate (*p*-SCN), and then attached onto lysine residue of HSA under weakly basic conditions. (E) The coupling molecule is modified to contain maleimide moieties, and then attached onto cysteine residue of HSA under weakly basic conditions.

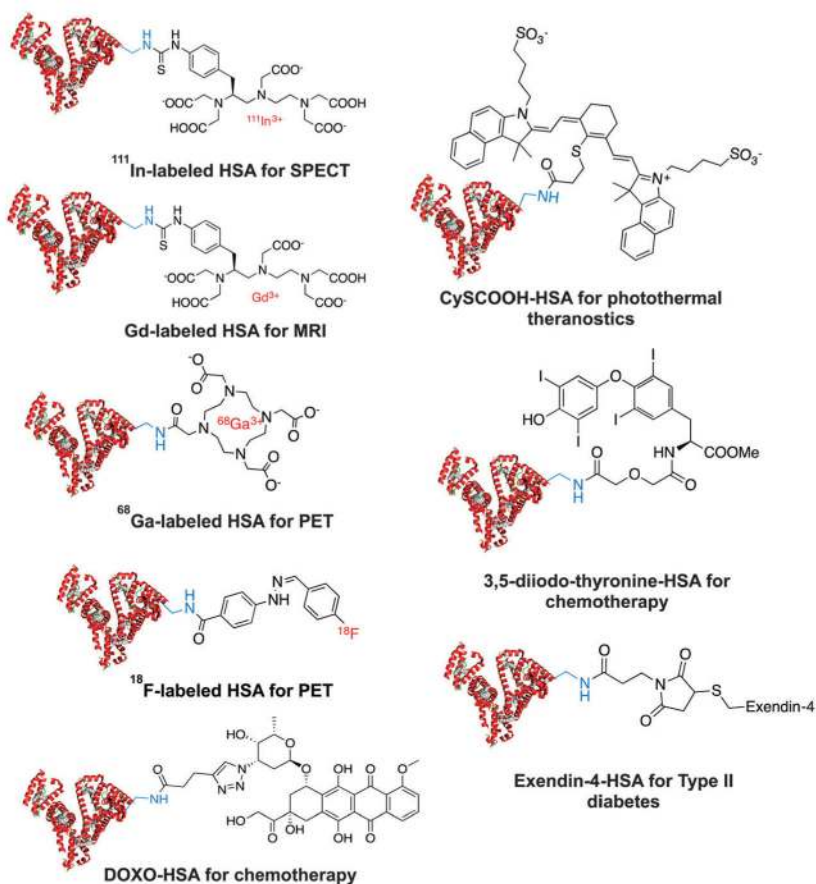


Fig. 2. Representative HSA drugs based on *in vitro* conjugation: (a) ¹¹¹In-labeled HSA for single-photon emission computed tomography (SPECT);⁵¹ (b) Gd-labeled HSA for magnetic resonance imaging (MRI);⁵² (c) ⁶⁸Ga-labeled HSA for positron emission tomography (PET);⁵³ (d) doxorubicin HSA conjugates for cancer chemotherapy with less side effect;⁵⁴ (e) ¹⁸F-labeled HSA conjugates for PET;⁴⁴ (f) CysCOOH HSA conjugates for photothermal therapy;⁵⁵ (g) 3,5-diiodo-thyronine HSA conjugates for antibody production in animals;⁵⁶ (h) exendin-4 peptide HSA conjugates for the treatment of type 2 diabetes.⁵⁷

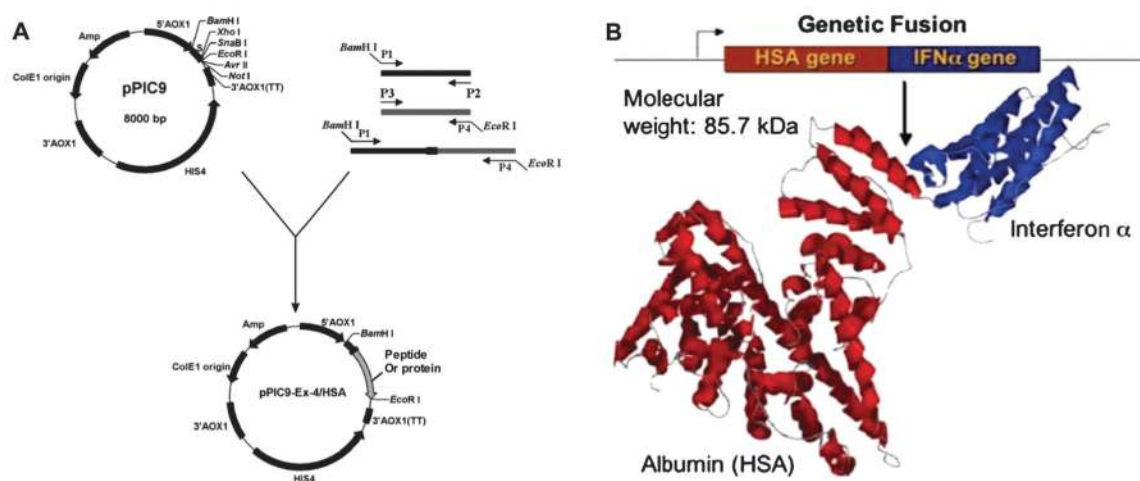


Fig. 3.
 (A) The construction of the recombinant protein that fuses HSA and a peptide of interest.
 (B) Schematic structure of a representative HSA fusion protein Albuferon. Reprinted with permission from ref. 58 and 4. Copyright 2007 (ref. 58) European Peptide Society and John Wiley & Sons, Ltd. and copyright 2008 (ref. 4) Elsevier B.V.

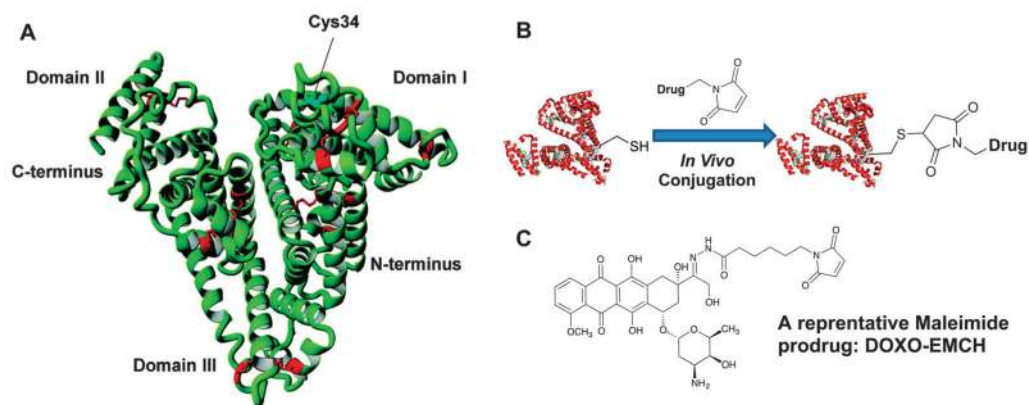


Fig. 4. (A) X-ray structure of human serum albumin in which the cysteine-34 position is marked as shown; (B) chemical structure of the (6-maleimidocaproyl) hydrazone derivative of doxorubicin (DOXO-EMCH); (C) a schematic description of *in vivo* thiol–maleimide conjugation.

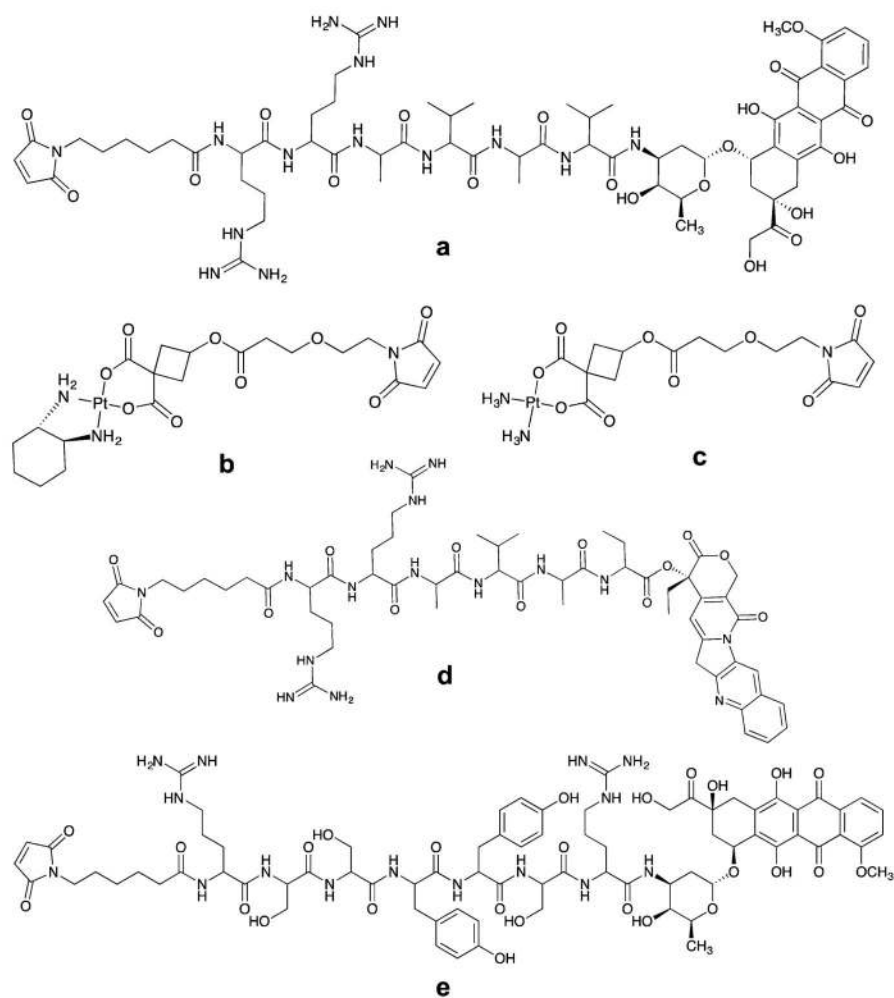


Fig. 5. Structures of selected albumin-binding maleimide modified prodrugs. (a) Doxorubicin prodrug that is cleaved by cathepsin B;⁷⁶ (b) and (c) albumin-binding prodrugs with Pt(II) complexes;⁷⁵ (d) camptothecin prodrug that is cleaved by cathepsin B;⁷³ and (e) doxorubicin prodrug that is cleaved by prostate-specific antigen (PSA).^{40,60,77,78}

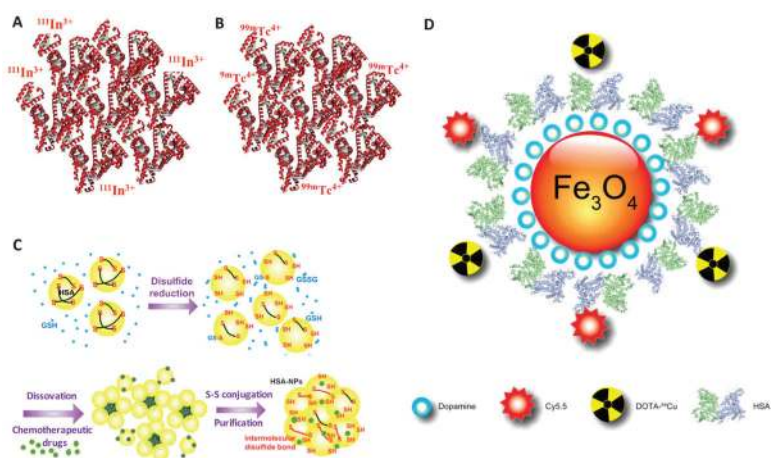


Fig. 6. Representative strategies of *in vitro* non-covalent HSA binding. (A) ^{111}In -labeled aggregated HSA for SPECT. (B) $^{99\text{m}}\text{Tc}$ -labeled aggregated HSA for SPECT. (C) Schematic description of the preparation of self-cross linked HSA nanoparticles. Reprinted with the kind permission from ref. 84. Copyright 2007 John Wiley & Sons, Ltd. (D) HSA coated iron oxide nanoparticles as multiple functional theranostic platform. Reprinted with permission from ref. 91. Copyright 2010 Elsevier B.V.

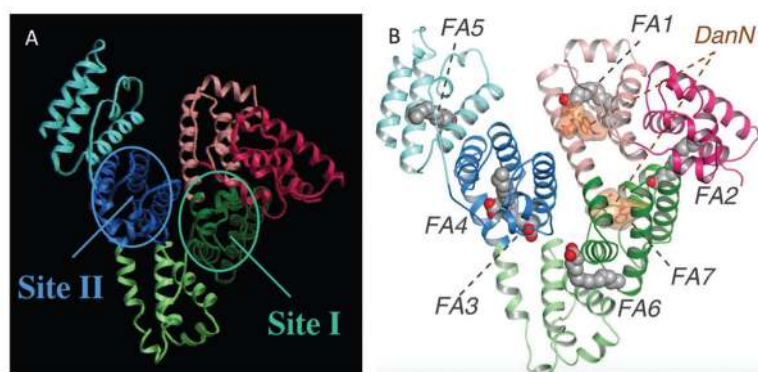
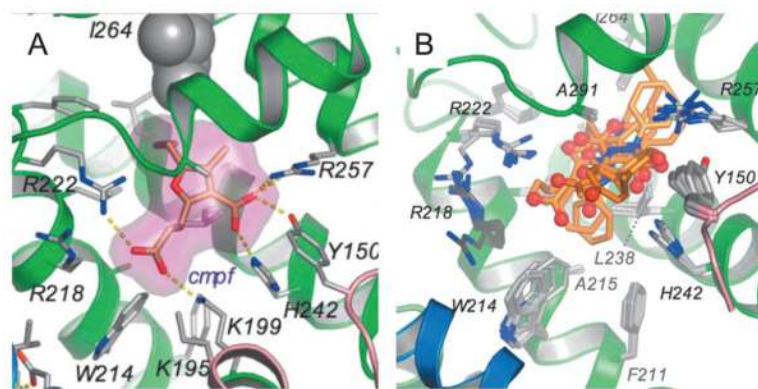


Fig. 7. Crystal structure of albumin illustrating (A) small molecule binding site 1 and site 2 and (B) fatty acid (FA) binding site.⁹³ Reprinted with the kind permission from ref. 93. Copyright 2005 Elsevier Ltd.

**Fig. 8.**

(A) Drug binding to site 1 in HSA (defatted). The detailed binding conformation is shown for 3-carboxy-4-methyl-5-propyl-2-furanpropanoic acid (CMPF), in which the drug is shown in a stick representation with a semi-transparent van der Waals surface. Sticks color-coded by atom type indicate selected side-chains; hydrogen bonds are shown as yellow dashed lines. (B) Top view of the superposition of CMPF bound to site 1 in defatted HSA. Drugs are presented as a stick model with carbon atoms colored orange, nitrogen atoms in blue and oxygen atoms in red.⁸⁵ Reprinted with permission from ref. 93. Copyright 2005 Elsevier Ltd.

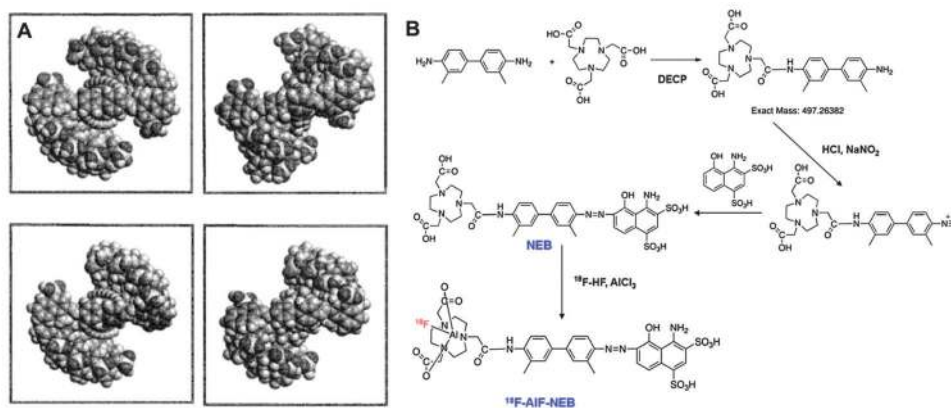


Fig. 9. (A) Schematic structure of supramolecular system of Evans blue that binds to the site 1 on HSA. As shown, Evans blue dye exhibits strong tendency towards self-assembly to form stable, continuous, ribbon-like supramolecules when it binds to HSA. This self-assembling capability is also found to essentially correlate with the capacity of protein binding;¹⁰² Reprinted with permission from ref. 102. Copyright 2000 John Wiley & Sons, Ltd. (B) Synthesis and ¹⁸F-AIF radiolabeling of NOTA(1,4,7,10-tetraazacyclododecane-1,4,7,10-tetraacetic acid)-truncated Evans blue conjugate (NEB).⁹⁹

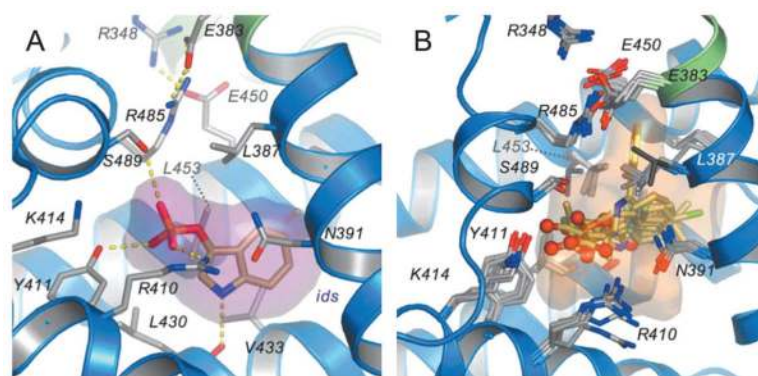


Fig. 10.

(A) Binding of indoxyl sulphate to site 2 in HSA. Indoxyl sulphate is shown in a stick representation with a semi-transparent van der Waals surface. Color-coding is the same as shown in Fig. 8. (B) Top view of the superposition of indoxyl sulphate bound to site 2 in HSA along with a semi-transparent surface.⁸⁵ Reprinted with permission from ref. 93. Copyright 2005 Elsevier Ltd.

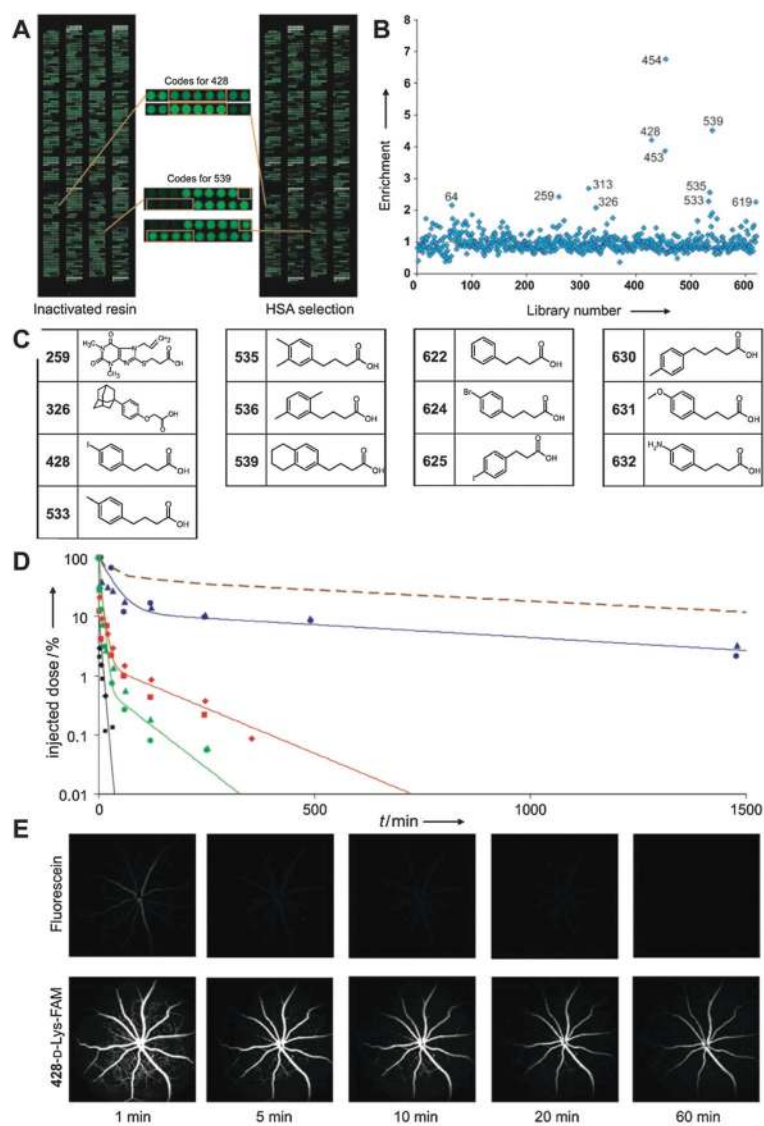


Fig. 11. (A) Microarray readout of the selections performed against inactivated resin and resin displaying HSA (right panel). The spots corresponding to the enriched compounds 428 and 539 are enlarged (center); (B) enrichment of compounds in selections for HSA binding (compound numbers are indicated). (C) Structures of the molecules identified as potential binders; (D) pharmacokinetic studies of fluorescein (black), 428-D-Lys-FAM (blue), 622-D-Lys-FAM (red), and phenethylamine-FAM (green) after injection in two mice each. As shown, the plasma concentration time course of ^{177}Lu -labeled MSA is listed here for comparison; (E) fluorescein angiography images in mice were recorded over 1 h after injection of 50 nmol of fluorescein (top row) and 428-D-Lys-FAM (bottom row).¹⁰⁴ Reprinted with permission from ref. 104. Copyright 2008 Wiley-VCH Verlag GmbH & Co. KGaA, Weinheim.

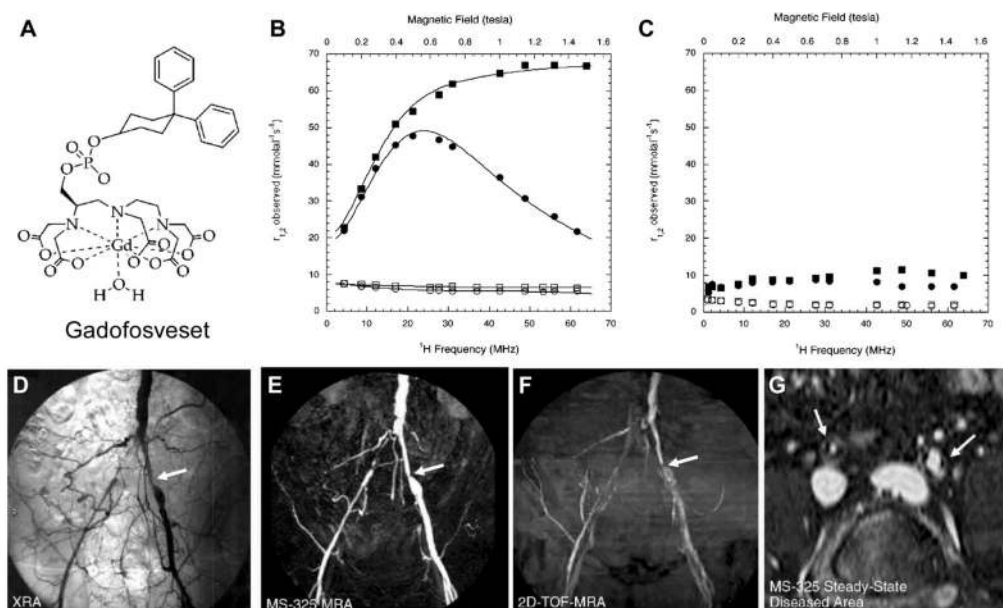


Fig. 12.

(A) Chemical structure of gadofosveset. (B) Observed longitudinal (r_1^{obs} , circles) and transverse (r_2^{obs} , squares) relaxivity for 0.1 mM gadofosveset in the presence (filled symbols) and in the absence (open symbols) of 22.5% (w/v) HSA at 37 °C, phosphate-buffered saline, pH 7.4. (C) Observed longitudinal (r_1^{obs} , circles) and transverse (r_2^{obs} , squares) relaxivity for 0.1 mM gadofosveset in the presence (filled symbols) and in the absence (open symbols) of 22.5% (w/v) HSA at 37 °C, phosphate-buffered saline, pH 7.4. Reprinted with permission from ref. 127. Copyright 2002 American Chemical Society (D–G) Comparable coronal projections of (D) conventional angiography, (E) gadofosveset enhanced MR angiography, (F) two-dimensional TOF MR angiography, and (G) a transverse reconstruction of a steady-state gadofosveset dataset showing stenoses (arrows) in both right and left common iliac arteries.¹³² Reprinted with permission from ref. 126. Copyright 2007 Radiological Society of North America.

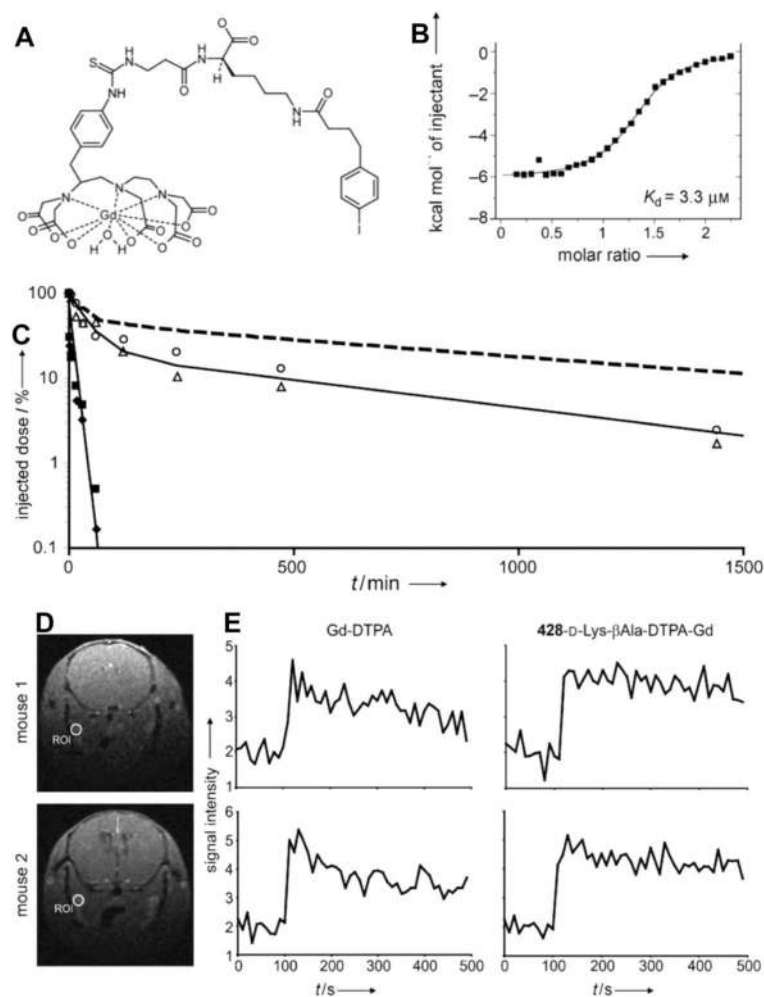


Fig. 13. (A) Chemical structure of 428-D-Lys-β-Ala-DTPA-Gd. (B) K_d value of 428-D-Lys-DTPA-Gd to HSA determined by isothermal titration calorimetry (ITC) at 37 °C. (C) Pharmacokinetic studies of DTPA-¹⁷⁷Lu (filled symbols) and 428-D-Lys-β-Ala-DTPA-¹⁷⁷Lu (empty symbols) after i.v. injection in mice. The plasma concentration time course of ¹⁷⁷Lu-labeled mouse serum albumin is given for comparison. (D) Transverse MR images of the mouse head indicating the region of interest (ROI) used to select the blood vessel. (E) Time course of the MR signal intensity in the ROI after injection of Gd-DTPA (left panels) and 428-D-Lys-β-Ala-DTPA-Gd (right panels).¹⁰⁴ Reprinted with permission from ref. 104. Copyright 2008 Wiley-VCH Verlag GmbH & Co. KGaA, Weinheim.

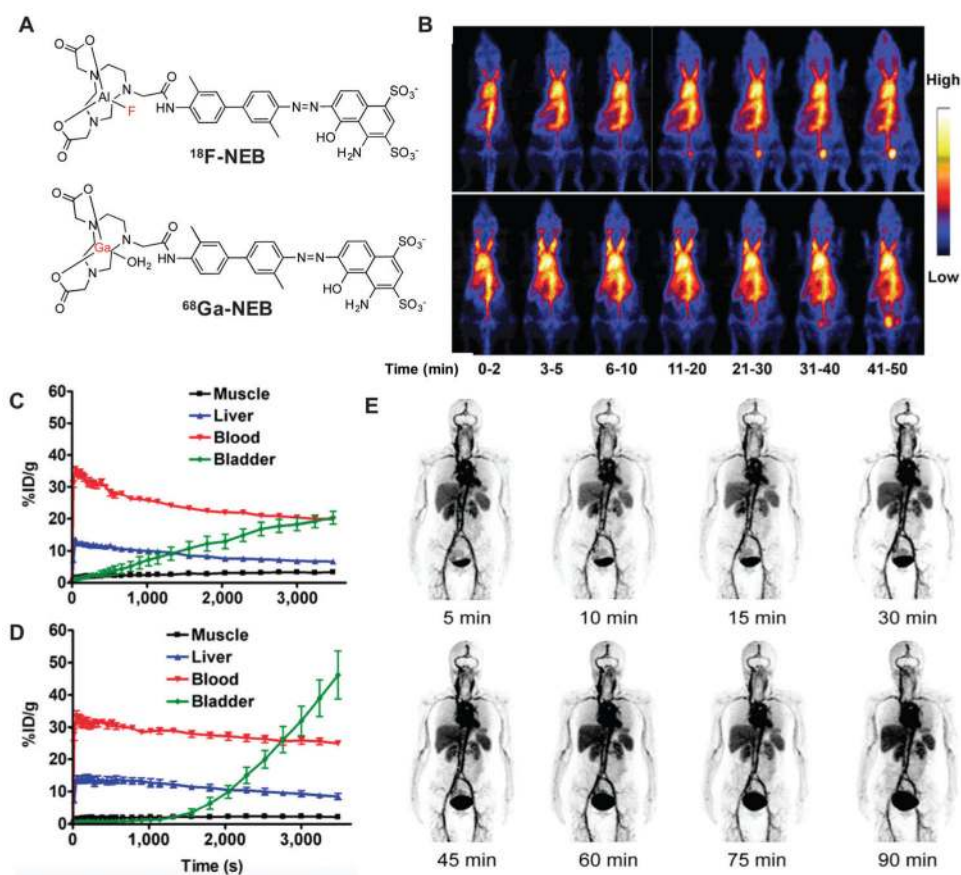


Fig. 14. (A) Chemical structure of ^{18}F -NEB and ^{68}Ga -NEB. (B) Series of maximum-intensity-projection PET images in normal mice after intravenous injection of either ^{18}F -AIF-NEB or ^{18}F -FB-MSA. Each mouse received around 3.7 MBq of radioactivity. Images were reconstructed from a 60 min dynamic scan. (C) Time-activity curves of ROIs outlined over muscle, heart, liver, and bladder regions on ^{18}F -AIF-NEB PET images. (D) Time-activity curves of ROIs outlined over muscle, heart, liver, and bladder regions on ^{18}F -FB-MSA PET images. Reprinted with permission from ref. 99. Copyright 2014 Society of Nuclear Medicine and Molecular Imaging. (E) Multiple time-point whole-body maximum intensity projection PET images of a female healthy volunteer at 5, 10, 15, 30, 45, 60, 75, and 90 min after intravenous administration of ^{68}Ga -NEB. Reprinted with permission from ref. 101. Copyright 2014 Society of Nuclear Medicine and Molecular Imaging.

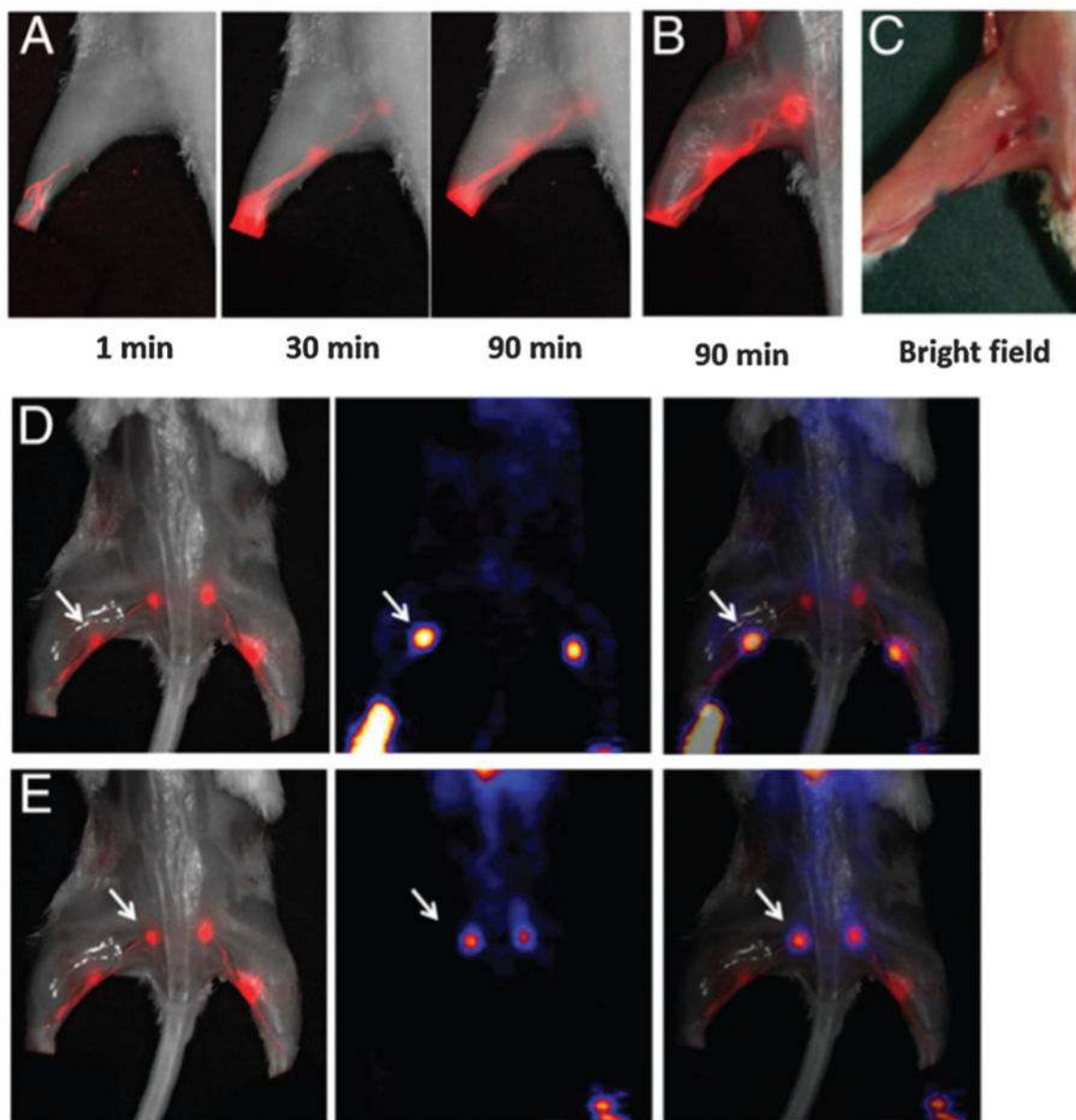


Fig. 15. (A) Longitudinal fluorescence imaging of the lymphatic system after hock injection of ^{18}F -AIF-NEB/EB. LNs and lymphatic vessels are clearly visible. (B) *Ex vivo* optical imaging of LNs without skin. (C) Photograph of the same mice to show the blue color within the LNs. (D) Co-registration of the optical image (left) and the PET image (Middle) to present the popliteal LNs, indicated by a white arrow. (E) Co-registration of the optical image (left) and the PET image (middle) to present the sciatic LNs, indicated by a white arrow. The mice were euthanized at 90 min after hock injection of ^{18}F -AIF-NEB/EB and the skin was removed.¹⁰⁰ Reprinted with permission from ref. 100. Copyright 2015 National Academy of Sciences.

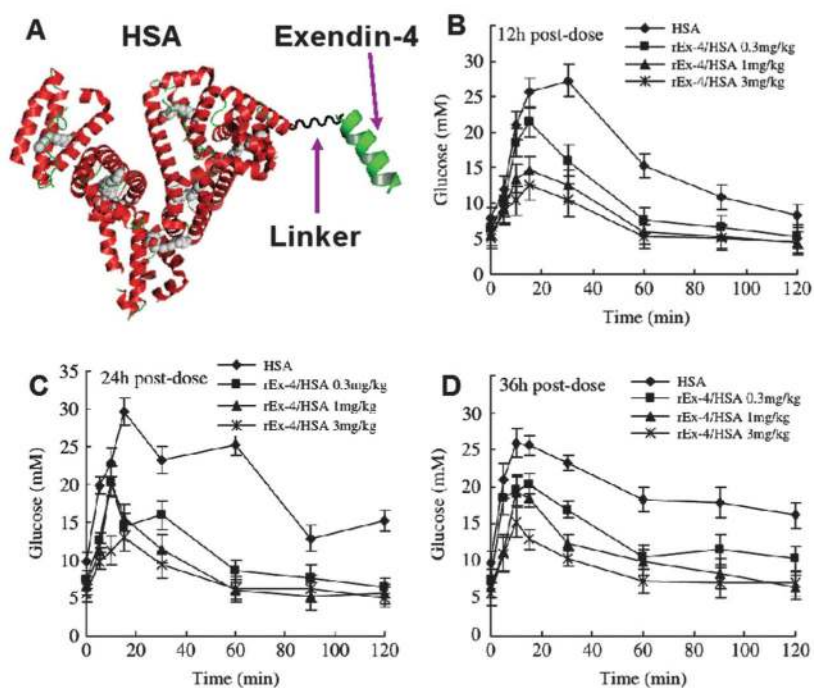


Fig. 16. (A) Schematic structure of E1HSA; (B) E1HSA lowers the blood glucose in db/db mice by an oral glucose tolerance test (OGTT). Single dose of E1HSA (0.3, 1, and 3 mg kg⁻¹) or HSA (3 mg kg⁻¹) were injected intraperitoneally in mice. OGTT was carried out at various times postdose to evaluate the duration of E1HSA action (B): 12 h; (C): 24 h; (D): 36 h. Values are expressed as means \pm SE; $n = 5$ mice per group.¹⁵⁸ Reprinted with permission from ref. 58. Copyright 2007 European Peptide Society and John Wiley & Sons, Ltd.

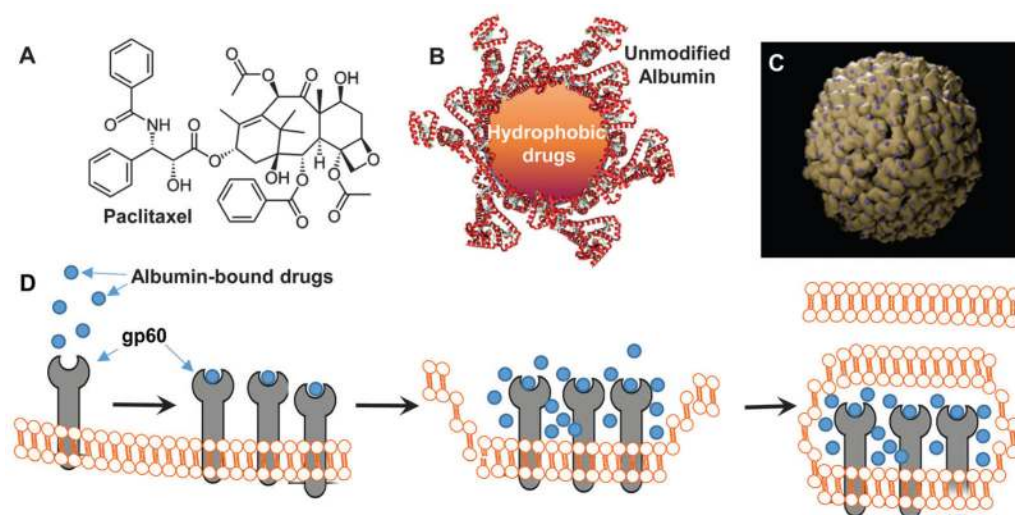


Fig. 17. (A) Chemical structure of paclitaxel, which is a hydrophobic small molecule with poor solubility in the blood. (B and C) Representative structures of small drug loaded albumin nanoparticles, and the diameters of this complex is between 80 to 150 nm with a mean value of 130 nm. Reprinted with permission from ref. 163. Copyright 2010 Elsevier B.V. (D) Process of gp60-mediated transcytosis of albumin across the vascular endothelium. The endothelial transcytosis of albumin is started by binding to the 60 kDa glycoprotein (gp60) receptor on the cell surface. This interaction induces caveolin and results in invagination and pinching off of the endothelial cell membrane, thereby concentrating and transporting the albumin complex into vesicular structures denoted as caveolae (“little caves”).

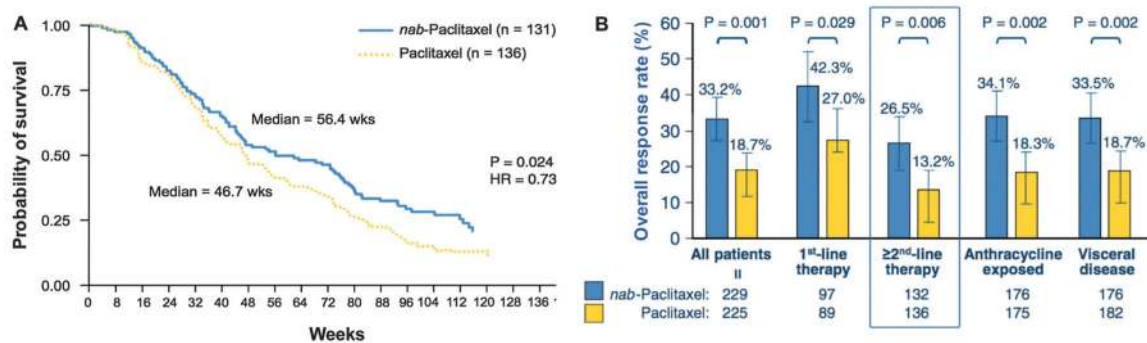


Fig. 18.

(A) Time to disease progression in a phase III comparative trial of *nab*-paclitaxel *versus* CrEL-paclitaxel. Reprinted with permission from ref. 164. Copyright 2005 American Society of Clinical Oncology. (B) Better efficacy of albumin-bound paclitaxel, compared with polyethylated castor oil-based paclitaxel in women with metastatic breast cancer. Reprinted with permission from ref. 163. Copyright 2010 Elsevier B.V.

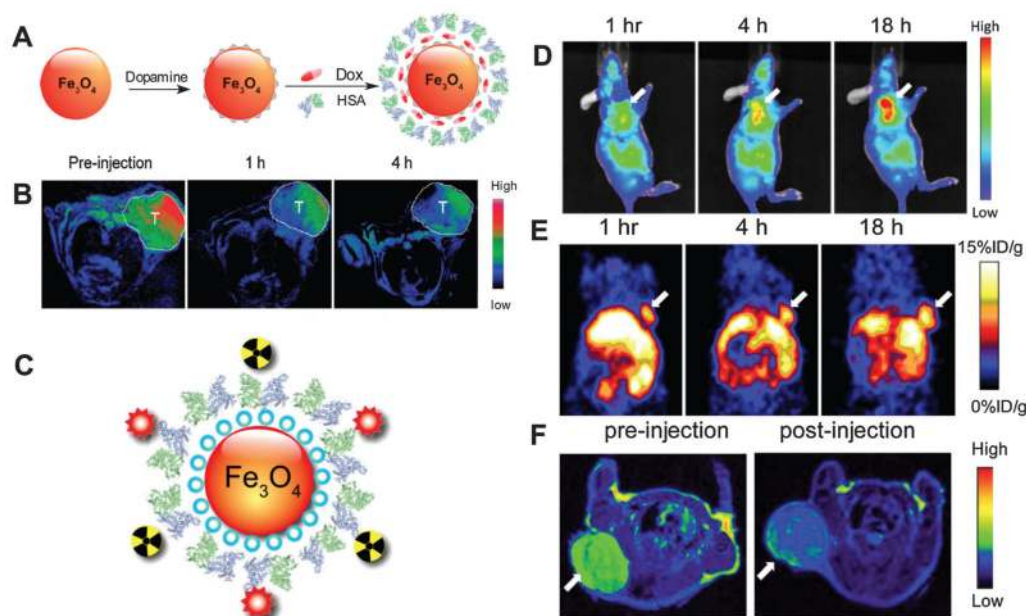


Fig. 19.

(A) A brief scheme to describe the preparation of albumin-coated IONP. Reprinted with permission from ref. 87. Copyright 2012 American Chemical Society (B) MR images taken before, and 1 and 4 h after the injection of NPs (6 mg of Fe per mL). As illustrated here, the contrast enhancement was decreased from 26.1% to 5.2% and then 4.3% at 0 h, 1 h and 4 h p.i., which was the result of tumor accumulation of HINPs. Reprinted with permission from ref. 87. Copyright 2011 American Chemical Society. (C) Schematic illustration of the multi-functional HSA-IONPs. (D) Representative *in vivo* NIRF images of mouse injected with HSA-IONPs. Images were acquired 1 h, 4 h and 18 h post injection. (E) *In vivo* PET imaging results of mouse injected with HSA-IONPs. Images were acquired by 1 h, 4 h and 18 hours of post injection. (F) MRI images acquired before and 18 h post injection.^{87,89,90,186} Reprinted with permission from ref. 91. Copyright 2010 Elsevier B.V.

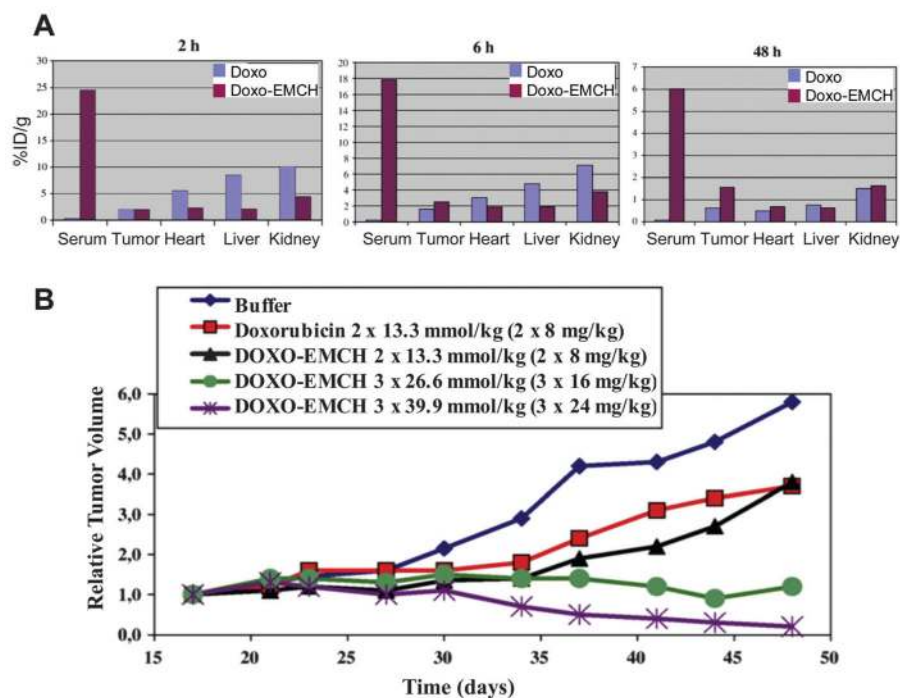


Fig. 20. (A) Biodistribution study in MDA-MB-435 xenografted mice with radiolabeled doxorubicin or DOXO-EMCH (organ values were corrected for blood volume); (B) curves depicting tumor growth inhibition of subcutaneously implanted MDA-MB-435 tumor under therapy with doxorubicin and DOXO-EMCH.^{188,189} Reprinted with permission from ref. 4. Copyright 2008 (ref. 4) Elsevier B.V.

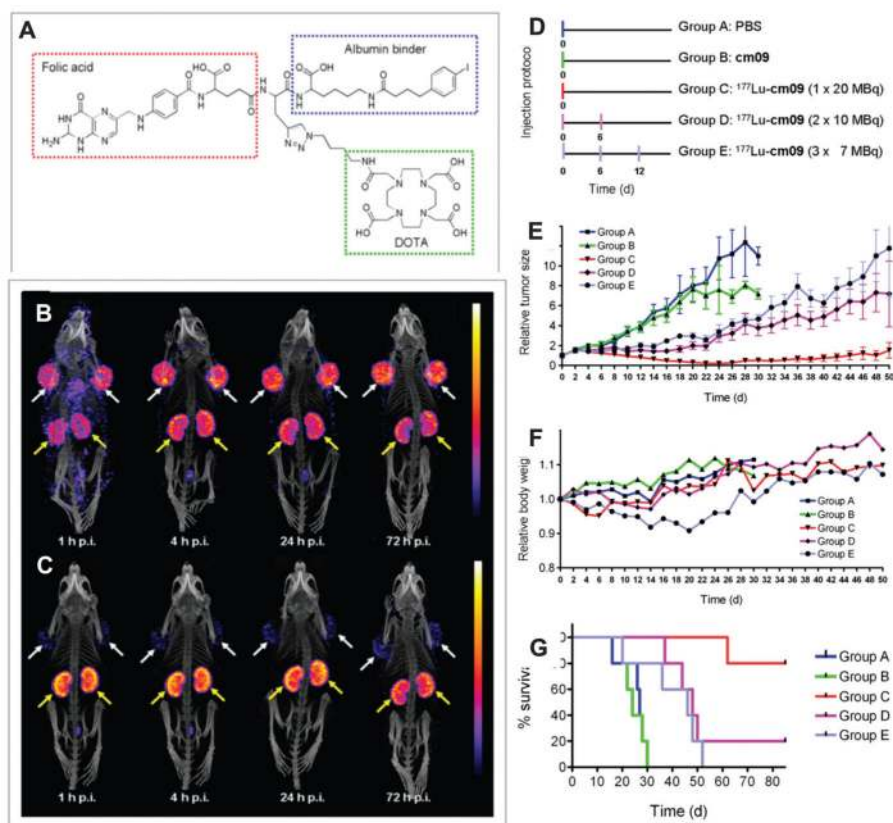


Fig. 21. (A) Chemical structure of cm09. (B and C) SPECT/CT images of KB tumor-bearing mice injected with ^{177}Lu -cm09 (B) and ^{177}Lu -EC0800 (C). Accumulation of radioactivity was found in FR-positive tumors (white arrows) and kidneys (yellow arrows). Images show a significantly improved tumor-to-kidney ratio (1.0 vs. 0.2) at 1, 4, 24, and 72 h after injection in mice that received ^{177}Lu -cm09, compared with mice that received ^{177}Lu -EC0800. (D) Internal radiation therapy protocol. (E) Average relative tumor size over time under different treatment regimens. (F) Relative body weight of mice under different therapies. (G) Survival curves of mice from groups A–E. (A, dark blue) control group. (B, green) unlabeled cm09. (C, red) 1×20 MBq of ^{177}Lu -cm09. (D, violet) 2×10 MBq of ^{177}Lu -cm09. (E, light blue) 3×7 MBq of ^{177}Lu -cm09.^{182,183} Reprinted with permission from ref. 210. Copyright 2013 Society of Nuclear Medicine and Molecular Imaging.

Table 1

A selective summary of clinically relevant HSA-based imaging agents and therapeutics^{4,10,20,24–27}

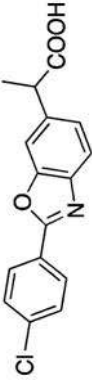
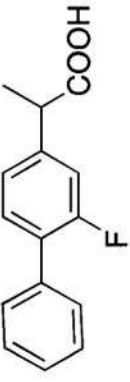
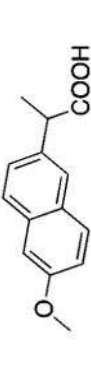
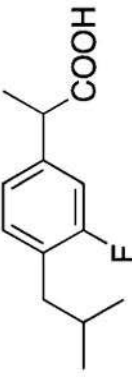
Company sponsoring clinical study	Brand name or drug code	Molecular type	Status	Indication of clinical studies	Clinical trial identifier number	Ref.
Novo Nordisk	Levemir	Fatty acid insulin conjugate	Approved	Diabetes	NCT00655044 NCT00806897	4
Novo Nordisk	Liraglutide	Fatty acid peptide conjugate	Approved	Diabetes	NCT01795248	4
GlaxoSmithKline	Albiglutide	Peptide HSA conjugate	Approved	Diabetes	NCT01357889 NCT00849017	160 and 161
Abraxis BioScience	Abraxane	Nanoparticle albumin bound small molecule	Approved	Breast cancer, lung cancer and prostate cancer	NCT01307891 NCT02027428 NCT00732836	4 and 167
Nycomed Amersham	Nanocoll	^{99m} Tc macroaggregated HSA	Approved	SPECT scan for breast cancer and rheumatoid arthritis	NCT00929032	20
Human Genome Sciences	Albinterferon	Interferon alpha (IFN- α) HSA conjugate	Phase III	Hepatitis C	NCT00724776	20
Innovive Pharmaceuticals	Aldoxorubicin	Doxorubicin maleimide conjugate	Phase III	Soft tissue sarcomas, small cell lung cancer	NCT01673438 NCT02235688	4
Conjuchem Inc.	CJC-1134	Peptide maleimide conjugate	Phase II	Diabetes	NCT01514149 NCT00638716	152
Fujisawa Deutschland GmbH	MTX-HSA	Methotrexate HSA conjugates	Phase II	Metastatic translational cell cancer	EORTC30951 EORTC20947	25

Table 2

Structure, binding affinity, number of binding for some classical binders to HSA binding site ^{193,96,97}

	<i>n</i>	Structure	<i>K</i> _d (μM)	Ref.
Benoxaprofen	2		33.1	93
Phenytoin	6		167	93
Bromphenyl blue	3		0.67	96
Evans blue	14		2.5	96
Phenol red	1		35.7	96

Table 3Structure, molecular length, binding affinity of some classical binders to HSA binding site ^{293,96,97}

#	Structure	Length (Å)	K_d (μ M)	Ref.
Benoxaprofen 1.0		14.7	3.2	93
Cicloprofen 1.1		13.2	52.1	93
Flurbiprofen 0.9		13.5	29.8	93
Ketoprofen 0.9		12.4	7.8	93
Narproxen 1.0		12.8	40.2	96
Ibuprofen 1.1		12.2	11.6	96


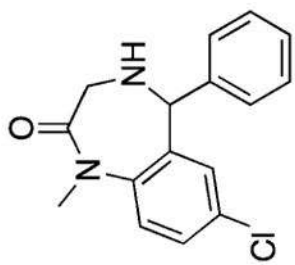

	<i>n</i>	Structure	Length (Å)	<i>K_d</i> (μM)	Ref.
Octanoate	1.0		13.1	1.8	97
Dazepam	1.0		14.6	2.6	96
Octylamine	—		13.4	—	93

Table 4Relaxivity for Ablavar and other gadolinium(III) complexes^{127,129–131}

Name	r_1 (mM ⁻¹ s ⁻¹)	Temperature (°C)	pH	Ref.
TREN-L-Me-3,2-HOPO	10.5	25	7.4	130
DTPA	4.3	25	7.4	131
DOTA	4.2	25	7.4	131
DTPA-bisamide	4.58	25	7.4	131
D03A	4.8	40	7.4	131
MP-2269	6.2	40	7.4	131
Ablavar	6.6	25	7.4	127

Author Manuscript

Author Manuscript

Author Manuscript

Author Manuscript

Summary of HSA-based blood glucose regulatory drugs. AUCs were extrapolated by the formula of $AUC = 1/2 \times [(2 \times \text{biological half-life value} + \text{peak time value}) \times \text{peak effect value}]^{20,57,113,152,160-162,211}$

Table 5

Sample	Chemical construction	$t_{1/2}$ (h)	CL/F (mL h ⁻¹ kg ⁻¹)	V_d (mL kg ⁻¹)	C_{max} (ng mL ⁻¹)	AUC (ng h mL ⁻¹)	MRT (h)	Ref.
Exenatide	Peptide	0.58 ± 0.09	861.2 ± 164.0	1534.8 ± 415.9	0.20 ± 0.06	0.39 ± 0.12	1.39 ± 0.15	20
Albugon	Peptide HSA perfusion	108 ± 13	14.3 ± 2.8	91.7 ± 13.6	614 ± 136	175 000 ± 37 000	94.8 ± 24.0	152, 160 and 161
E1HSA	Peptide HSA perfusion	56.7	2.1	102	N.A.	206815.9	66.7	162
E2HSA	Double peptide HSA perfusion	53.4 ± 8.0	1.66 ± 0.27	125.5 ± 8.8	1810.1 ± 198.7	179182 ± 27 148	78.3 ± 6.2	57
LUA-MI	Peptide fatty acid conjugates	4.0 ± 0.5	6.61 ± 2.06	38.87 ± 15.30	892.66 ± 249.31	6940.4 ± 2571.5	7.85 ± 0.32	113
Ex-PEG (5 kDa)	Peptide PEG conjugates	6.1 ± 0.8	37.5 ± 13.5	310 ± 79.1	76.1 ± 14.5	101.0 ± 25.8	7.9 ± 0.3	211
Ex-PEG (20 kDa)	Peptide PEG conjugates	49.4 ± 7.7	4.4 ± 0.4	272.9 ± 63.2	154.0 ± 5.3	893.5 ± 119.3	53.1 ± 0.6	211
Ex-PEG (40 kDa)	Peptide PEG conjugates	76.4 ± 7.4	2.3 ± 0.3	259.0 ± 61.6	148.1 ± 24.5	1780.7 ± 279.9	78.9 ± 0.4	211